Shapes in Motion: Confotronics , Tanglotronics , Animotion

Igor M. Kulić

13.2.2018

Contents

Preface

This text is about shapes in motion. More precisely, it is about how shapes give rise to their own motion. When I look back at the work reviewed here, to my own defense I can only say that I was mainly guided by an aesthetic feeling of beauty of shapes in motion.

Why are we, as humans, so naturally attracted to moving shapes? Of course it is hardwired in our genes - our very survival depends on understanding and predicting the patterns of shapes in motion around us. The corresponding endorphine rush inside our pleasure centers is genetically programmed, as much as the one for love.

That at least is what science says, stealing the last hideouts of mystery, crunching it , turning it into knowledge and technology. Luckily, while mystery is always on the run, it never really disappears. It merely migrates, feeding on our mental capacity to perceive it in some other spot.

In this picture here you see what mystified me for years.

Figure 1: Kaleidocycle: A paper object able of moving inside out in an "impossible" way.

It mystified some other people before as well. Its inventor, Paul Schatz, called it "der umstülpbare Würfel" and first turned its motion into technology by making a mixer out of it. M.C. Escher, reshaped it into its final geometry. He also made it stunningly beautiful and known to the rest of the world by putting his "Escher tilings" on it. After having a brief, coincidental encounter with this object in the 1990-ies I have experienced a puzzling, spiritual feeling, that in some distant future I will understand and harness it for a new technology. In the years that followed I have periodically revisited the object in my memory. For long I could not remake it or figure out what it was (before Internet emerged), but I always found myself drawing energy from the memory of our first encounter.

Now, I am not sure if I understood this object right. In order to make it more ideal and beautiful (to my senses), I smoothed it out and eliminated all of its edges. What remained in my mind was a smooth toroidal object, but one undergoing a smooth, continuous motion - a constant flux along its surface. Later on I managed to recreate this animated motion -"animotion"- and built working engines that realized it. I will tell you more about these engines , called "animas" and their "animotion" in Chapter 3.

You will also find animotion ,in a disguised form, within the collective "wobbling mode" of microtubules (Chapter 1). Somehow, ironically, that kaleidocycle, from Fig. 1, infected my thinking and all I could ever come up with was a (veiled) realization of it, wherever I looked. But I am fine with that, because of all the pleasurable adventures and sidetracks I experienced on the way there.

Talking of pleasure , you might be surprised to hear that both shape and motion are born out of frustration. If there were no conflicting forces, and no stresses acting on a thing - at least transiently- it would not start moving. Nor would it take any other shape than that of a sphere (or a random blob). Of course the concept of frustration is not merely poetic , but has some very

concrete meaning in physics. To be specific, by frustration I mean the inability of an object to reach its preferred state (e.g. free energy minimum) in the context of a conflicting surrounding that prevents it from doing so.

In the following, I promise you shapes, some motion, a bit of delightful frustration and at the end we will together "reinvent the wheel" and embed it inside of a material. If you bear with me and follow the slightly ridiculous invitation, I promise a hilarious, but meaningful resolution of this outrageous claim.

Outline

Shape and motion are born by frustration.

Computation is a son of a switch.

If there is any single thread in this manuscript (beyond subjective aesthetics), then it is to create active, information processing objects with all their functions intrinsically woven and encoded within their fabric. There are three main directions of thinking, pointing towards complementary technologies, that will be in our focus in the following Chapters (1-4). I nicknamed them "confotronics" , "tanglotronics" and "animotion". Hoping to convince you that they are not only worth calling names but also worthwhile studying, let me explain what I mean.

Confotronics (Chapter 1) deals with the interaction of elastically and conformationally switchable units. It originates from studies of switchblade biological lattices - like switchable monomers in bacterial flagella or microtubules. Though it might sound far fetched, my main reason for studying confotronics is its potential to realize tiny, synthetic nano-axons, carrying conformational information pulses, and bridge between polymer physics and self-organized artificial intelligence.

Unlike confotronics which is concerned with elastic and geometric couplings between units, **tanglotronics** (Chapter 2) deals with a topological coupling between them. More concretely, in its current realization, it describes how active entanglement generating units change the properties of polymeric materials like active gels and rubbers. The main current aim of tanglotronics is towards active materials and shape-invariant topological nano-machines.

Finally **animotion** (Chapter 3) is a surprising, active, frustration and topology driven motion of an "embedded wheel" within the material. If you find this cryptic, just hold on to see the "fiberdrive" in the last section. I am sure you will be somehow delighted, at least by the "hot-spaghetti-motor" and "fish-line-loop-motor", inventions that you can try out at home. In this context we will ask the questions: Is it possible to merge the wheel and axle into a single element and embed the mechanism into the material? And can we build rotary engines out of a *single piece* of responsive material?

Surprisingly, the answer to both questions is an enthusiastic: Yes!

In the last Chapter 4 we finally conclude with an outlook on the ongoing and future projects.

Chapter 1

Soft Confotronics

This first Chapter deals with the newly emerging field of what I tentatively call "confotronics". In itself it presents the basic skeleton of a unified approach to soft switchable lattice systems in biology. Our basic idea is to learn from Nature and eventually make our own synthetic confotronic systems for information processing and transmission in the future.

1.1 The Toolbox of Confotronics

Soft confotronics is the investigation of conformational states of large assemblies of soft switchable units, typically bio-molecules forming regular functional superstructures. Through their interaction, the discretely switchable individual monomer units give rise to new complex phenomena, only present in the assembled superstructures and perform biological tasks that a single unit cannot.

A large zoo of confotronic systems is found in the living cell, where allosteric protein assemblies like viral capsids and filament lattices collectively switch states (and shapes) due to their complex mechanical inter-monomer interactions. The biggest plethora of confotronic examples is found in classical biological filaments: For instance DNA bases can flip , tilt and interact with the orientation of the sugar phosphate backbone , giving rise to discrete "A", "B" and "Z" forms of DNA. These DNA states are highly cooperative and are "copied" from one base-pair to the neighbors.

It is a bit less known that besides the genes, the cytoskeleton is the second vast playground of confotronics. Microtubule's elementary units (tubulin dimers) act as curvature switchable elements [47] and actin filaments can switch their inter-unit twist [31]. The propensity for unit multistability in these cases seems to be encoded in monomer's molecular complexity (rearranging hydrogen bonds and ion bridges). However , even some very generic interactions along the backbone like tail bridging (cf. below), or geometrical constraints including confinement to surfaces[95] can break the symmetry and uniqueness of filament's

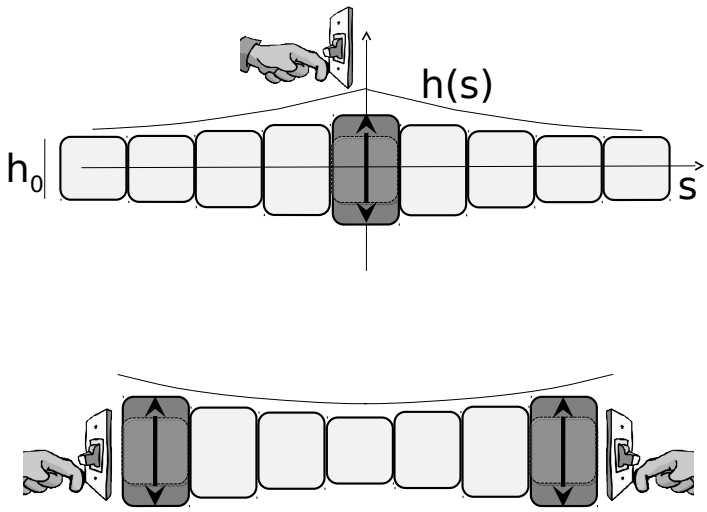

Figure 1.1: Problems of confotronics: propagation of conformational information and inter-unit coupling

ground state. In many cases multistability cannot be simply averaged out on biologically relevant scales (nanometers to microns) especially when strong positive cooperativity between the units comes into play. This in particular means that many aspects of such switchable filaments cannot be described with simple, classical models of semiflexible polymers ("worm like chains").

At this point , one could naturally ask if we can somehow view confotronic phenomena in a unified manner. Can we crystallize out basic principles and identify an essential "toolbox of confotronics"? Staying away from atomistic details we shall look for a picture that is more conceptual and coarse grained in spirit, yet still detailed enough to get an idea how to *rebuild* confotronic systems synthetically in not so far future from now. In its spirit the theory of confotronics developed here attempts to go beyond the common phenomenological models of cooperative units [101, 102] where the type and sign of interactions are a priori *assumed*. Instead, ideally confotronics aims at *predicting the interactions*, from known (elastic) forces in the system. We might not completely succeed at this point with the purest form of this program. Yet the aim of eliminating arbitrary *ad hoc* assumptions and applying an elastic coarse-graining approach shall at least be stated here.

When it comes to general principles, there seem to be a few basic motifs and laws that govern most of confotronics.

Maybe the most basic principle can be stated as:

Principle 0: Neighboring units conformations *cannot not* interact!

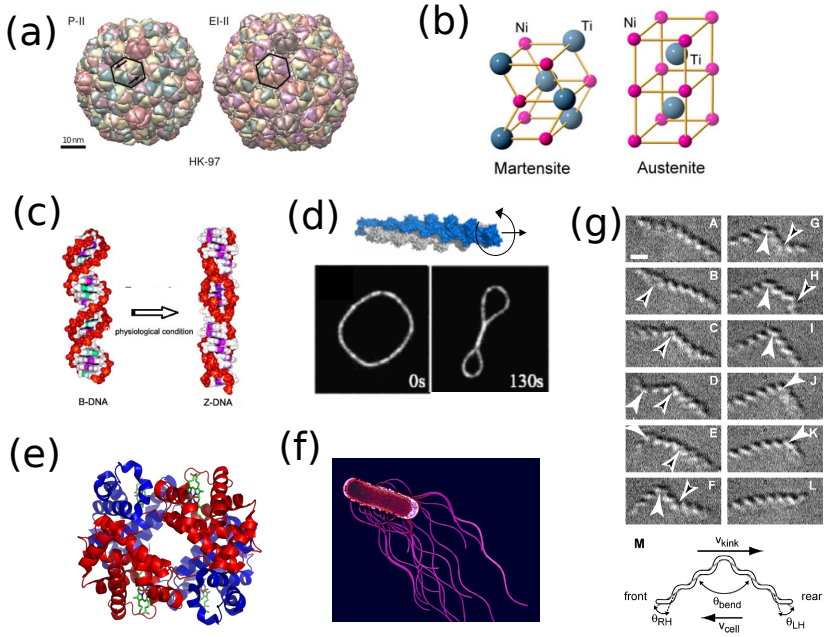

Figure 1.2: Examples of confotronic systems in (living and dead) Nature: a) Viral capsid proteins switch conformation and undergo collective rearrangements. b) Shape memory alloys undergo collective lattice transitions upon temperature change. c) At high salt DNA can dynamically switch from right to left handed form (B->Z -DNA switching). d) Actin monomers undergo angular switching leading to actin ring supercoiling. e) hemoglobin tetramers undergo cooperative switching to bind oxigen in sigmoidal fashion. f) Bacterial flagellin filaments undergo cooperative ("polymorphic") transitions to helical states. g) The minimalistic bacteria spiropasma undergo active conformational transitions of their cytoskeletal sheet (found on the inside of their membranes). By undergoing a yet unspecified lattice switch that induces a right-left-helical kink and actively propagates along their body they manage to rapidly swim. This is the only documented example of a an active/dissipative confotronic machine.

Although this statement feels somehow trivial ,at first glance, it is deeply encoded in the nature of the mechanical interaction. It says that it is not possible to reshape one unit without affecting an other neighboring one in some way. Switching/reshaping units can either promote or inhibit the switching of their neighbors , depending on geometry. This inevitable interaction is however only important on larger scales if a second requirement is fulfilled. The second principle seems to be:

> Principle 1: *Nature is digital*: monomer units are (frustrated) bistable switches.

Bistability, i.e. the existence of two or more discrete states of the units is a basic motif. Confotronic molecular units behave a bit like a mechanical light switch and toggle between two (or more) well defined states. In this mechanical analog there is a hidden component called "spring toggle mechanism". It combines a spring with a bunch of hinges to generate bistability of the mechanism. Like in the light switch, also in Nature, it is crucial that the spring and the other parts of mechanisms are in mechanical conflict i.e. in *frustration*. Biological filaments are often equipped with stressed polymeric backbone cross-linkers that display similar features to its mechanical analogue. Nature seems to be frustrated and "digital" in a similar way.

> Principle 2: *Anisotropy* steers easy signaling directions

To tune how one switch affects the neighboring one Nature very often tends to weaken elastic variables along some specific directions so that the conformational signal can travel along this "easy" direction. Anisotropy and bistability synergistically superimpose to increase the interaction strength to very large distances.

> Principle 3: Geometric constraints induce *variable sign* interactions

Principle 0 states that there is always some form of interaction, yet the *sign and the strength* of this interaction are not specified a priory. It appears that most interactions are "generically" cooperative i.e. have a positive in sign , as Monod ,Wyman and Changeux have correctly recognized for symmetry reasons [101]. But this is only one side of the coin and the full story is much more interesting. To obtain anti-cooperative interactions Nature can use tricks by introducing certain global geometric constraints. If the geometry is right, switching "on" one unit can lead to the switch "off" of another unit somewhere far away.

> Principle 4: Global constraints lead to *collective variables*

By using topological tricks Nature can create soft collective variables - so called zero elastic energy modes (ZEEMs) - that even in absence of explicit anisotropy couple many monomers together. The monomers tend to lose their individuality and immerse into a global soliton like excitation.

In the following we will illustrate these basic principles with some conceptual examples. From them one can build a rather general and functional "theory of

confotronics" of which we present only some anecdotal fragments. A sketched outline of how a confotronic model (in a simple 1D medium) works, starting from elasticity to active autowaves (akin action potential in neuronal axons) can be found in the Appendix A.

1.1.1 Non-Linearity and Frustration : The Confotronic Flip-Flop

On the molecular scale -with all its (bio) chemical repertoire of interactions- it is rather easy for Nature to generate bistable elements. But how can bistability appear on a more coarse grained level, e.g. of larger molecules or continuous materials? The short answer is through a nonlinearity and mechanical frustration.

One particularly ubiquitous motif is something that we could call the "confotronic flip-flop". It consists of an arrangement of two non-linear units that are not individually switchable (monostable units) but when "glued" together they become collectively bistable. We can think of it as a tri-layered structure with two outer layers which individually prefer a contracted state and a middle layer which is inextensible. When such a structure bends with a centerline curvature κ to one side there is a contractile/tensile strain of the order $\varepsilon \approx \pm\kappa d$ where d is the distance between the centerline and the outer layers. The $\pm$ refers to two different layers depending on which sign the (signed) curvature κ. If both outer layers are identical and have the same energy given by $g(\varepsilon)$ then the total energy is simply their sum $g_{tot}(\kappa d) = g(+\kappa d) + g(-\kappa d)$ .Such a system become bi-stable when g_{tot} has a maximum at κ i.e. $\frac{\partial g_{tot}}{\partial \kappa}|_{\kappa=0} = 2\frac{\partial g}{\partial \kappa}|_{\kappa=0} < 0$. This implies a convexity of g i.e. $\frac{\partial g}{\partial \kappa}|_{\kappa=0} < 0$. Remarkably, a bi-stability of g is not really required , only its convexity around zero - a significantly weaker requirement. Further below we will see some examples but one could note that many systems when they consist of at least two non-linear and inflicting units could exhibit bi-stability.

1.1.2 Emergence of Bistablility and Cooperativity in a Filament

Another, more concrete example for frustration induced bi-stability is a semi-flexible filament decorated with elastic "tails"cf. Fig. 1.3. These tails span along filament's surface and pairwise connect distant points at some typical distance d. Let's say that they have some spring constants k (per unit length), and the filament's central core (backbone) has a bending stiffness B. When the filament is straight, the springs are in their extended (prestressed) state with length d and and have an energy $E_{ch} \sim \frac{1}{2}kd^2$. The core, on the other hand, with its bending energy $E_{bend} = \frac{1}{2}B\kappa^2$ is still in its ground state with vanishing curvature $\kappa = 0$. If however , the chains become overextended they have the tendency to buckle the filament at the expense of bending the backbone. It is easy to work out the filament undergoes a buckling transition form once

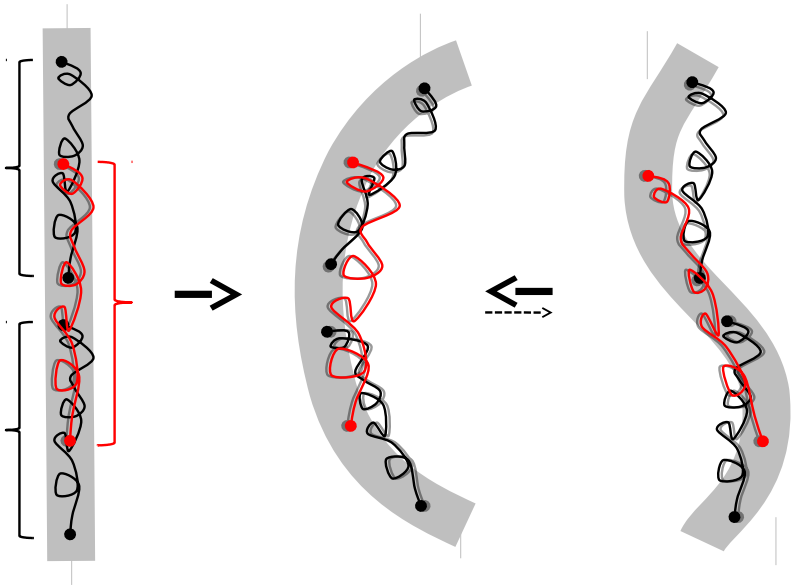

Figure 1.3: a) A semiflexible filament with elastic tails that cross-link points along its backbone becomes bistable. If the cross-linking point intervals overlap in addition (red chains) the curvature switching becomes cooperative.

the chains become too extended $k > k_{crit} = 12Bd^{-3}$. Close to the buckling transition $k \gtrapprox k_{crit}$ and on length scales $\gg d$ the energy can be expanded as

$$E_b \approx \frac{kd^3}{2} \int \left[C_1 \left(\frac{k_{crit}}{k} - 1 \right) \kappa^2 + C_2 d^2 \kappa^4 \right] ds$$

with C_1,$C_2 > 0$ numeric constants. Such a system is bistable and displays curved sections of with switchable curvature

$$\kappa \propto (\pm) \frac{\sqrt{1 - k_{crit}/k}}{d}.$$

If the chains attachment interval do not overlap the curvature switching is local and non-cooperative on distances larger then d. However , in the more generic case when they do overlap (cf red chains in Fig. 1.3) it is easy to see that there is an additional cooperative coupling term emerging

$$E_{couple} \approx \frac{H}{2} \int \kappa'^2 ds \tag{1.1}$$

with $H \propto kd^5$ a higher order "hyper-stiffness" constant. Note that the latter gives rise to a *persistence of curvature*, rather than the usual persistence of tangent angle (as in common semiflexible chain models).

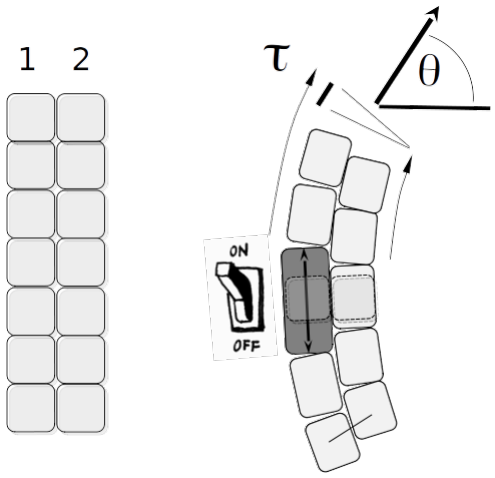

Figure 1.4: Two filaments are coupled with elastic springs forming a simple two chain bundle. The shear and bending degrees of freedom become strongly coupled and lead to long range deformation effects.

This rather neat toy model is less academic than one would think. Classical biofilaments , like microtubules have naturally built-in long amorphous polymer tails that can span in their stretched state to nearest neighbors or beyond. Furthermore , actin filaments and microtubules often interact with other polymer tail forming proteins that come as integral part of the cytoskeleton (calledf "tau" proteins, "MAPs", "formins" etc.). Switchability, in particular of microtubules might partially relate to the tails.

1.1.3 Anisotropy

Let's now have a look how elastic anisotropy comes affects interactions and consider again a simple model [92, 93, 94], cf. Figs 1.4: two glued together, semiflexible filaments that are cross-linked by soft spring connections. In addition to the bending energy per length $\sim B\theta'^2$, with $\theta(s)$ the tangent angle at position s and B the bending stiffness (twice that of of a single chain), there is also an inter-chain shear deformation, call it $\tau(s)$. The latter gives a second elastic contribution, the shear energy $\sim K\tau^2$. For our simple two filament bundle of lateral width w, the elastic shear constant is given by $K \sim w^2 k$ with the elastic spring constants k (per unit length) of the individual cross-linking connectors. The total energy can then be written as

$$E = \frac{1}{2}\int B\theta'^2(s) + K\tau^2(s)\, ds \tag{1.2}$$

In the limit where the axial stretching of the two filaments can be neglected

the shear deformation at any given location s along the contour can be expressed in terms of θ

$$\tau(s) = \theta(s) - \bar{\theta} \tag{1.3}$$

with the average angular orientation

$$\bar{\theta} = L^{-1} \int \theta(s)\, ds.$$

The energy 1.2 with the constraint 1.3 can be interpreted (for weak angular deformations $\theta \ll 1$) as a that of a semiflexible filament under strong (internal) "tension" K [94]. The latter is quite peculiar as it is not applied from the outside but rather behaves as an internal "self-tension" that acts with respect to the mean internal orientation $\bar{\theta}$. This gives rise to long range curvature-curvature interactions. For instance it is easy to see that if a fixed curvature κ_0 is imposed within a certain arc region of length l around some position s_0, it will automatically induce opposite curvature in its proximal regions, cf Fig. 1.4 b. Far away from s_0 the shear and bending deformations decay exponentially

$$\theta' \propto \tau \sim \kappa_0 l \exp(-|s - s_0|/l)$$

with a characteristic screening length scale set by

$$\lambda = \sqrt{B/K}.$$

If the arc is short, $l \ll \lambda$, its total energy

$$E_{arc} \sim \sqrt{BK}\kappa_0^2 l^2$$

scales quadratically with its length in contrast the more classical semi-flexible chain models where $E_{arc} \propto l$. For longer fixed curvature arcs the shear energy dominates over bending and grows even quicker with $E_{arc} \sim K\kappa_0^2 l^3$. Each piece of the arc interacts with any other one in a non local manner and it becomes increasingly costly to form longer arcs (the energy density E_{arc}/l grows in a size dependent manner). This striking non- extensivity of energy is a signature of curvature cooperativity along the chain.

1.1.4 Global Constraints: Positive and Negative Cooperativity

The simple example from previous section violates the Monod-Wyman-Changeux (MWC) [101, 103] rule of thumb that suggests that interactions are (generically) positive for symmetry reasons. The interactions between two same curved regions above are in fact *competitive* rather than cooperative. Contrary to the common belief allostery in a symmetric arrangement of identical subunits can be both positive or negative. The sign of interaction strongly depends on local and global geometry of the system. A somehow typical example for how the interaction can flip sign can be seen in Fig. 1.1.4. Such and similar schematic

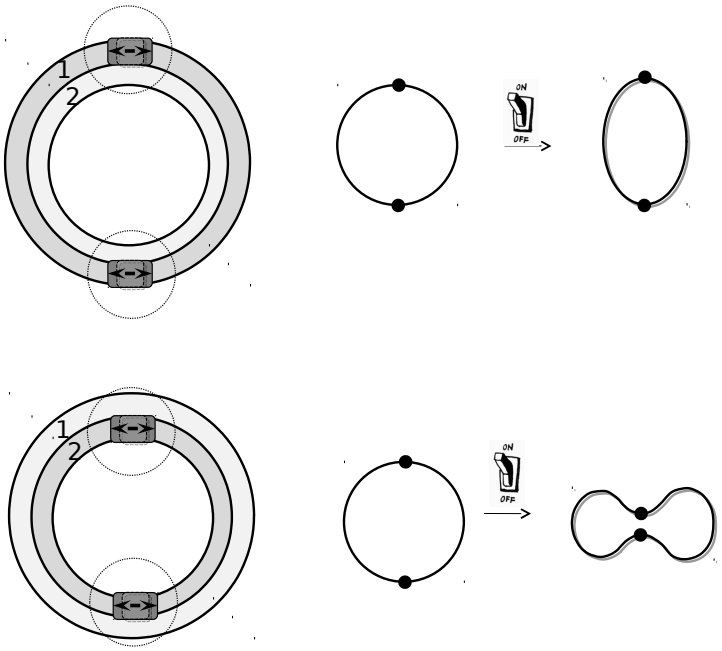

Figure 1.5: The sign of interaction depends on the geometry. Top row: If the two switches are in the outer filament (1) they cooperate. Bottom row: When they are on the inside they compete.

models with global coupling and negative cooperativity can be found in [96]. A more interesting and realistic system with variable sign of interaction - the switchable microtubule model [47, 48, 97, 46]- we will discuss in the following section.

1.2 Microtubule Confotronics

After this excursion in general , but rather simplified principles of confotronics, let's have a look at a concrete example from Nature: the microtubules.

Microtubules are cytoskeletal protein filaments of eukaryotic cells fulfilling different structural and mechanical functions in the cell: microtubules act as "cellular bones" strongly influencing the cell shape, constitute the main routes for molecular motor mediated intracellular cargo transport [49, 50] and perform other important tasks like stirring the cytoplasm [51]. Besides, they play a central role in the assembly of the mitotic spindle during cell division and are at the heart of the functioning of cilia and flagella [52]. This versatility of microtubules in a variety of biological functions mainly relies on their unique high stiffness and on their dynamics of assembly and disassembly. The high rigidity of microtubules (similar to hard plastic) is due to their structure that is known in exquisite detail from 3D electron microscopy reconstructions [53, 54] : microtubules are hollow tubes whose walls are formed by assembly of a variable number of parallel protofilaments (linear stacks of tubulin dimer units, abr. by PFs). The PFs themselves are built by head-to-tail self association of the $\alpha\beta$-tubulin heterodimer protein subunit (yielding a polarity to microtubules) whose structure has been resolved by electron crystallography [55, 56].

They have been in biophysical focus for several decades but the confusing and mutually contradicting results regarding their elasticity have shed some doubts on their understanding in the framework of classical semiflexible models. At the current stage the switchability of its elementary subunit (the tubulin-dimer) offers the simplest explanation for the observed complexity [46, 47, 48]. The principal result of such a "confotronic theory" of microtubules is that they can spontaneously form large scale cooperative superhelices of micron size pitches and diameters. The cooperativity of fluctuating internal degrees of freedom in combination with the cylindrical microtubule symmetry, that gets broken by an instability, lead to a helical state with very unique characteristics in the world of macromolecules. One of them is that microtubules can have a degenerate ground state and permanently reshape even if we grip them by the ends [47, 46]. A second implication is that microtubules can switch conformations when acted upon sufficiently large forces and torques[48]. According to the confotronic model they can then live in kinetically stabilized, metastable states which are mechanically strongly altered and bear very large curvatures (of the order of inverse microns).

We will outline the confotronic microtubule model from an elementary perspective. The reader interested in the more differentiated biological details we refer to the review article[47].

1.2.1 Microtubules as Anisotropic Lattices

A first theoretical attempt to cope with some aspects of the microtubule mechanical complexity was the "soft shear model" (SSM) or "anisotropic composite material model" [80, 84, 93, 94]. In this model the microtubule is considered as a mechanically anisotropic structure [80, 84] with the tubulin protofilaments acting as strong fibers that are rather weakly mutually linked with easily shearable inter-protofilament bonds. Some specific equilibrium statistical and mechanical properties of the SSM were investigated in [93, 94].

Although, in detail it does not reproduce all the experimental anomalies[47] the model has some nice physical features. In particular it develops a linear response theory of switchable (or binding) proteins along an anisotropic lattice. The model predicts how the binders/switches distort the lattice and thereby mutually interact at a larger distance (up to a ˜micron). Any local lattice deformation gives rise to a long distance curvature relaxation [94] and can lead to a long range interaction along the microtubule contour (cf. the anisotropic-toy-model from previous section). This aspect of the "soft shear model" is in phenomenological agreement with cooperative deformations induced by enzymes like katanin. Interestingly, the model also predicts a length-dependent persistence length which approximately resembles the measured behavior [84, 85].

1.2.2 Microtubules as Switchable Lattices

While the soft shear model does bring in some cooperativity / non-locality in the description of microtubules it does not fully account for all the findings. In fact a mounting experimental evidence points toward a higher degree of complexity: an intrinsic curvature switch of the microtubule lattice.

A model for spontaneous microtubule curving behavior was proposed in [47, 46] and later extended to active motor induced curving in [48]. In a nutshell, in such a model the tubulin dimer is treated as a bistable entity and modeled by a two state variable $\sigma_n(s) = 0, 1$ which corresponds to the straight and curved state at each lattice site. The $n = 1, ...N$ is the circumferential protofilament index (N is typically 10-15) and $s \in [0, L]$ is the longitudinal position variable along the MT centerline.

The model is based on the following assumptions:

(I) The tubulin unit (dimer) fluctuates between 2 states - straight and curved - with an energy difference $\Delta G > 0$ favoring the curved state (see Fig. 1.8). The energy density resulting from the switching of tubulin dimers is then given by

$$e_{trans}(s) = -\frac{\Delta G}{b} \sum\nolimits_{n=1}^{N} \sigma_n(s)$$

with $b \approx 8nm$ the dimer unit length.

(II) There is an Ising type nearest-neighbor cooperative interaction of units states *along* the protofilament axis with an interaction energy $J > 0$ favoring nearest neighbor units (on the same protofilament) to be in the same state. This

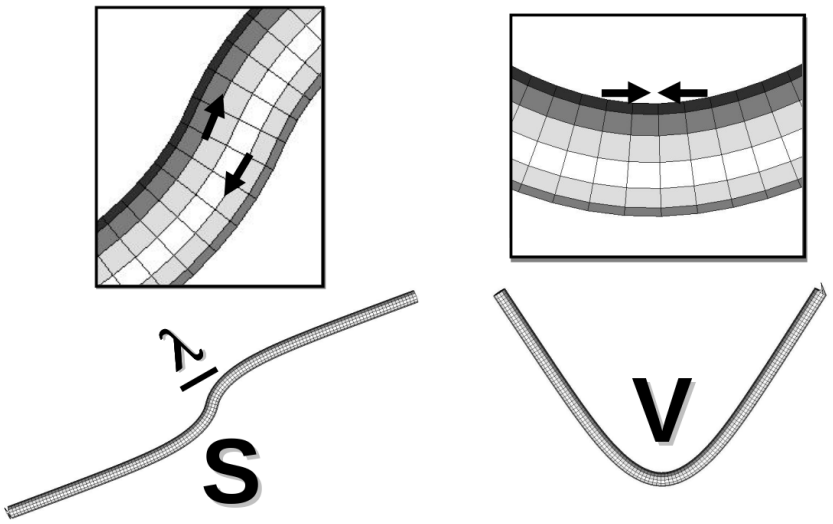

Figure 1.6: Two types of elementary deformations on the microtubule lattice : The S-let inducing a shear deformation that produces an S-shaped microtubule lattice deformed over a length scale λ that depends of the lattice elastic constants. A V-let is a compressive/tensile deformation along the microtubule axis and produces a V-like deformation - a kinked shape curving over the distance λ.

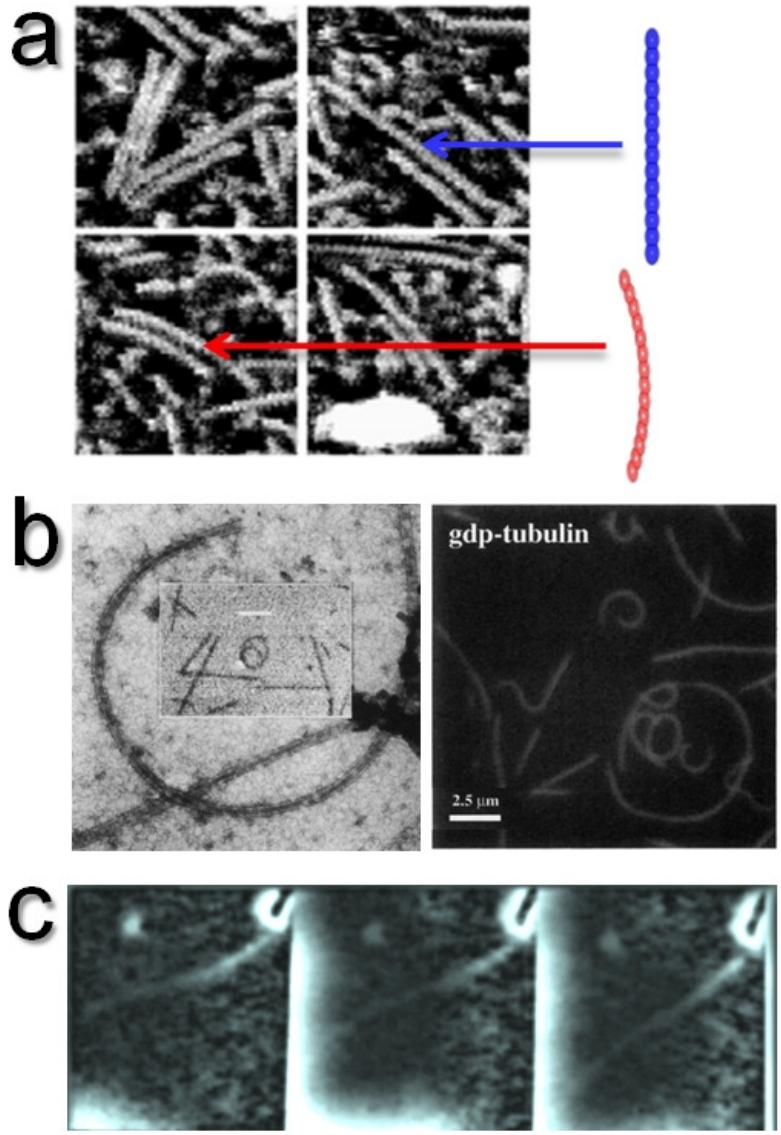

Figure 1.7: The empirical evidence for tubulin bistability: (a) A single taxol stabilized protofilament can coexist in a straight and a slightly curved state (reproduction from [72]) (b) Microtubules in gliding assay experiments can switch to a stable circular state and move on circular tracks (from [89][90]). Microtubules are occasionally observed to switch back and forth between the circular and straight states. (c) End-attached microtubules form a three-dimensional helicoid structure with a $15\mu m$ pitch (from [74]).

leads to the interaction energy density of the form

$$e_{inter}(s) = -(J/b)\sum_{n=1}^{N}(2\sigma_n(s)-1)(2\sigma_n(s+b)-1)$$

.

(III) Finally the microtubule lattice is also an elastic medium associated with an elastic energy density. The material strain deformations ε are related to the centerline curvature vector $\vec{\kappa}$ via $\varepsilon = -\vec{\kappa}\cdot\vec{r}$ with $\vec{r}$ the radial material vector in the cross-section. For a swichtable lattice the actual deformation energy depends on the switching-induced preferred strain ε_{pre}. It can be written as

$$e_{el}(s) = \frac{Y}{2}\int_{R_i}^{R_o}\int_{0}^{2\pi}(\varepsilon-\varepsilon_{pre})^2 r dr d\alpha$$

where the integration goes over the cross-section with R_i and R_o the inner and outer microtubule radii respectively. The prestrain $\varepsilon_{pre}(s,r,\alpha) \sim \pm\varepsilon_{PF}\sigma_n(s)$ is a function of the switching state σ_n and the induced prestrain on the protofilament level ε_{PF} (see Fig. 1.8). The latter can be extracted from experiments to be $\varepsilon_{PF} \approx 10^{-2}$. Collecting all energy contributions together the total elastic + polymorphic energy of the MT is then given by

$$E_{MT} = \int_0^L (e_{el} + e_{trans} + e_{inter})\, ds. \tag{1.4}$$

The ground state such a model can be determined by the interplay of the first two terms e_{el} and e_{trans}. The last term e_{inter} rules over cooperativity and determines how uniform the lattice states are along the microtubule contour.

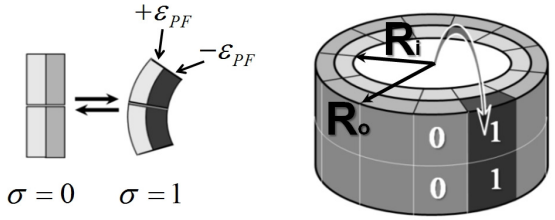

Figure 1.8: Strains and deformations in the polymorphic tube model. Each tubulin dimer can fluctuate between a straight state $\sigma = 0$ and a curved state $\sigma = 1$ of intrinsic curvature κ_{PF}. The curved tubulin dimer generates a positive prestrain $+\varepsilon_{PF}$ on its inner part and an equal but negative prestrain $-\varepsilon_{PF}$ on its outer part.

There are two interesting consequences of this model that we should mention in passing (more details are in the attached papers). The first is that microtubules under certain conditions can exhibit large scale helical ground states.

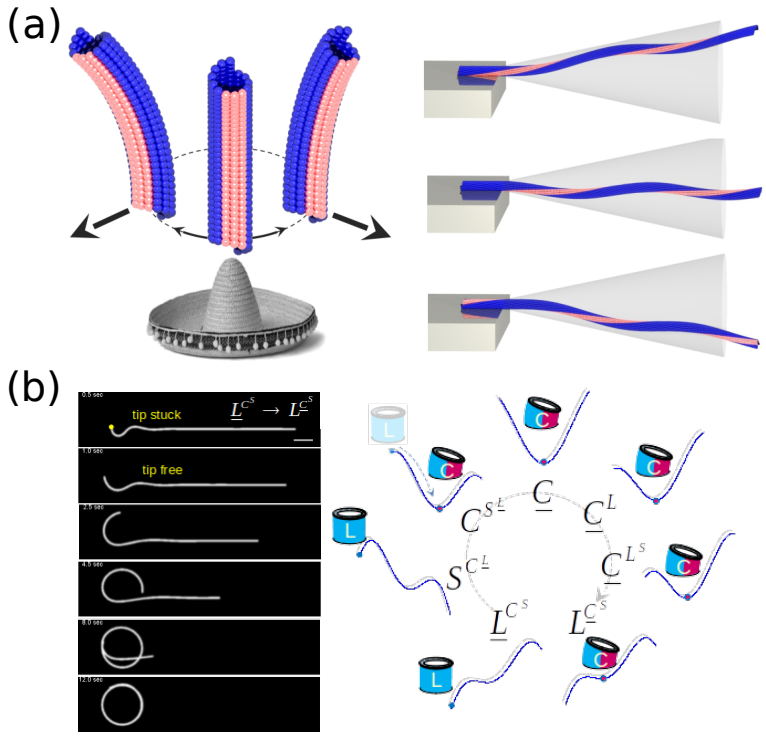

Figure 1.9: Interesting consequences of the switchable microtubule model: A) The helical zero energy mode of a clamped microtubule. B) Curvature switching and hysteresis when microtubules glide on kinesin motor carpets.

Most notably these ground states, that correspond to different orientations of the helix, are degenerate and the microtubule can hop between them. The corresponding effective potential looks like a Mexican hat, see Fig 1.9. The elastic zero-mode resulting from such a potential, gives rise to a collective (thermal) rearrangement dynamics that might confuse any experimenter trying to measure the microtubule persistence length or investigate its elastohydrodynamic relaxations.

The second , very notable consequence is that microtubules can forcibly switch from a straight into a curved state when molecular motors act upon them [48]. When bent by an external torque and then released again , they can end up in a metastable , highly curved state. In this more elaborate model the Mexican-hat potential becomes concave around zero and has a rather deep dimple at its top that competes with the ridge states (i.e. curved lattice states) at the hat perimeter. In spite of this metastability, the curved microtubule state can still persist for several minutes until it relaxes again to the initial straight tube state.

1.2.3 Variable Sign Interactions and Collective Zero Modes

The mentioned models of microtubules fit smoothly into our initial paradigm of a confotronic polymer in that there are switchable units (or conformation-modifying, lattice-binding entities) represented by a binary state variable $\sigma = 0, 1$. Now, unlike in the initial simpler cases, microtubules are more than 1-d lines. Topologically they are more of a cylinder, parametrized by the arc-length s and an azimuthal angle ϕ. This second variable makes microtubule confotronics much more interesting than that of a line. The switching variables$\sigma(s, \phi)$, which are now a function of two coordinates s and ϕ are coupled in an interesting an more complex way than in the 1-d case. It turns out that the coupling energy between two points on the surface, (s_1, ϕ_1) and (s_2, ϕ_2) , is of the generic form

$$E_c \sim -\exp\left(-\frac{|s_1 - s_2|}{\lambda}\right) \cdot \left|e^{i\phi_1}\sigma(s_1, \phi_1) + e^{i\phi_2}\sigma(s_2, \phi_2)\right|^2 \qquad (1.5)$$

The first, exponentially decaying term is intuitive. The decay length along the microtubule contour, λ depends on the concrete form of the theory (i.e. on coupling terms like J, elastic constants of the lattice, etc) but the exponential form of the decay is no surprise. The real interesting thing is the second term which says that the individual switches interact as complex numbers. These complex entities have an amplitudeσ and a phase $e^{i\phi_1}$ set by their azimuthal position on the lattice. If we rotate them all by another angle $\Delta\phi$ and transform them like $\sigma(s, \phi) \to \sigma(s, \phi + \Delta\phi)$ it has no influence on the interaction energy. This of course is the "Mexican hat", zero energy mode described above.

The sign of the coupling is also interesting. If the units switch to the same state on *the same side* of the lattice ($e^{i\phi_1} \approx e^{i\phi_2}$) , they tend to *cooperate*. If they are on the opposite sides they cancel each other ($e^{i\phi_1} \approx -e^{i\phi_2}$) and thus *compete*. This naturally leads to a clustering of switched units on one side of the lattice and to a broken symmetry and lattice curvature.

On a more course-grained, the superposition of the discrete switches gives rise to a collective "polarization" variable attached to each cross-section

$$P(s) = \sum_{n=1}^{N} e^{i\phi_n}\sigma(s, \phi_n)$$

where $\phi_n = 2\pi n/N$ and N the number of units at each cross-section. The polarization P can be seen as an embedded vector pointing perpendicular to the microtubule axis along the Frenet- normal to the centerline. The emergent microtubule curvature κ is proportional to the polarization's magnitude $\kappa \sim |P|$. The rearrangement of the polarization P (and thus the curvature κ) we have previously called the "wobbling mode". It is probably the hallmark signature of a whole class of frustrated confotronic models on tubular lattices. It relates to the toroidal ZEEM (zero elastic energy mode) that we utilize as an active "embedded wheel" to make novel machines in Chapter 3.

1.3 Outlook

In this Chapter we have outlined a tentative framework for soft confotronics based on some concrete examples. For a more mathematical walk-through the methods (on a concrete 1D example) see also the Appendix A at the end. The thinking we have developed here should help us to go beyond a pure description of biological systems into a practical utilization and fabrication of synthetic confotronic systems[1].

[1]These could one day transmit and process information on the molecular scale. The synthetic confotronic fiber - a man made filament of interconnected switchable units- when coupled to an external source of energy could behave rather similar to our brain's neuronal axons. This analogy , that we are currently pursuing in experiments could some day lead to synthetic axons transmitting confotronic signals at large speeds on nano-scopic scales. Thoughts and projects on our lab grown, DNA based nano-mechanical units and confotronic fibers of them are outlined in the last Chapter.

Chapter 2

Tanglotronics

We have seen how confotronics deals with geometric and elastic communication of units. Going beyond geometry, it is sometimes desirable to establish a less rigid and "more forgiving" coupling between nanoscopic units. By "more forgiving" I mean that two units that we couple to each other need not be in any particular, exact geometric arrangement to be able to communicate. Take for instance a usual copper conductor, coupling between some electronic elements in a circuit. For the mutual interaction of the elements, it does not matter how we move around a resistor, capacitor or transistor in space and bend the conductor as long as the wire connectivity is the same. Confotronics does not have this feature a priori built in : e.g. bending a microtubule changes the state of the monomers and their interactions. The field of mathematics dealing with structural "forgiveness" (or shape invariance) is called topology. In the following we will develop the concept of tanglotrons -topologically coupled active units that perturb the topological state of a polymeric material and consequently induce actuation on the macroscopic scale.

2.1 Nano-Motors and Polymer Entanglement

Many rotary engines exist in Nature [3] with the most prominent examples being the ATP-synthase [4, 5], the flagellar motor of bacteria [6] and various DNA- topoisomerases [7]. Also several artificial directed rotors based on various operational principles have been developed [8, 9, 11, 10, 3] and new rotary engine designs continue to be proposed and light up our imagination in nano-engineering [12, 2].

Thus Nature "knows" and "makes" molecular motors. Remarkably, it also utilizes polymer topology for eons as well. Living organisms naturally harness the principle of topological energy storage in our genomes [7, 29, 30, 29]. DNA double strand untwisting energetically shifts the threshold for DNA opening and activates genes. DNA untwisting (negative supercoiling), also provides an additional energy source for chromosome folding and compaction throughout

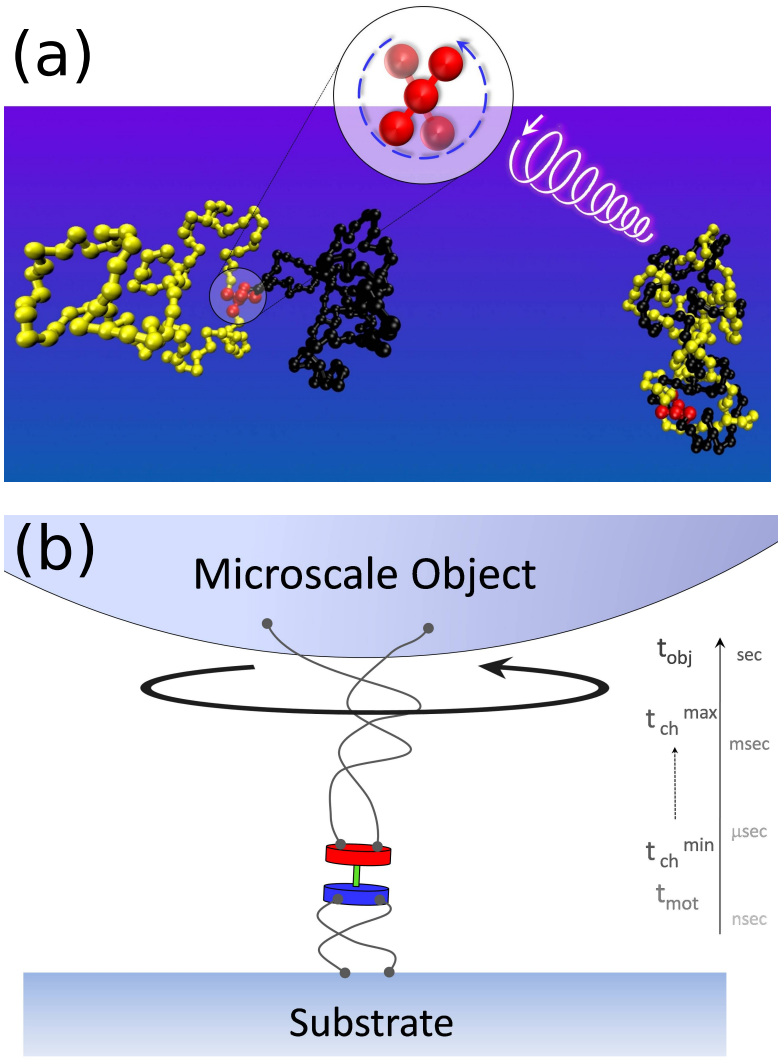

Figure 2.1: The tanglotron principle and its utility: a) The operation of the rotary motor is coupled to polymer chains. They entangle and spatially collapse causing volume change and mechanical actuation. b) Direct coupling of a molecular motor to a much bigger object is generally difficult , inhibiting the motor's operation. However, using the soft, topological coupling via polymer chains enables the operation of the motor and actuation (rotation) of the bigger object to decouple in time and happen at their individual characteristic timescales.

the living realm.

Now , lets say we have a functioning molecular motor at our hands, for instance a synthetic one like the Feringa's rotary photo engine [10], and we want make it perform a useful task on its environment. One can think of many ways of coupling a rotary unit to its surroundings - in theory. But in practice any hard , rigid coupling tends to suppress the kinetics and strongly affects the practical functionality of the nanomotor. This is because , synthetic molecular motors (including the Feringa motor) are delicate entities that easily jam or break when *rigidly* coupled to anything much bigger than them. The central idea presented here, is to attach soft polymer chains to the device, capture and conserve the motor generated rotations by topology. This in a nutshell is what I call the **tanglotron** unit. An active rotary (nano)motor coupled to a number of polymer chains buffering and storying the energy of motor rotation.

2.2 Topology and Actuation of Tanglotron Units

A tanglotron is cyborg-hybrid between an active rotary motor unit and a passive polymer entanglement unit. The original idea [41] is related to the concept of molecular motors operating in closed DNA ring geometries [2]. As there is no other practical way to couple such DNA rotary engines with the rest of the world, attaching polymer side chains for topologically harnessing motor rotations seems a logical necessity. The evolution of the initial idea [41] eventually ended in the collaboration with an experimental group and the synthesis of the first dynamically entangling polymer ("tanglotron") gel [42], see Fig. 2.2.

To understand how and why these gels contract we dive a bit into conceptual theory. In a nutshell , when polymer chains, having a finite length and thickness , are forced to wind around each other many times, they "run out of length" for larger excursions and thus tend to compactify. In this process of entanglement they lose their configurational entropy and thus act as free energy storage.

Of course there is quite a large body of theoretical knowledge about polymers entanglement (in thermal equilibrium). In fact, entanglement and its effect on the visco-elasticity of polymer networks is *the* classical problem in polymer science [13, 14, 15]. In a usual polymer melt, spontaneous, thermally induced polymer entanglements are created and destroyed in a dynamic fashion, by the so-called process of polymer "reptation". During mechanical shearing of a dense melt of long polymers, the relaxation of transient polymer entanglements is also the main cause of dynamic stress relaxation [13, 14, 15]. So in a sense, the concept of dynamic, transient entanglements is at the core of polymer physics.

The other classical problem, of fixed ,statically frozen-in, topological entanglement has also attracted a lot of theoretical interest. A number of simplified, two dimensional [16, 18, 17, 19, 20] and less tractable three dimensional models [21, 22] for the entanglements of flexible polymer chains have been developed in the past. Motivated by single DNA molecule probing experiments [23] applying torques on the molecular scale by magnetic tweezers, the problem of DNA supercoiling [24], DNA braiding [26] and its untwisting [25] has been studied

Figure 2.2: Tanglotron concept [41] and its realizations [42]: a) A tanglotron nano-gel consisting of only two chains attached to a Feringa motor. b) Contraction of a tanglotron gel in simulation and experiment. The gel collapses upon fueling the nano-motors (via UV light) by a factor 8 in volume.

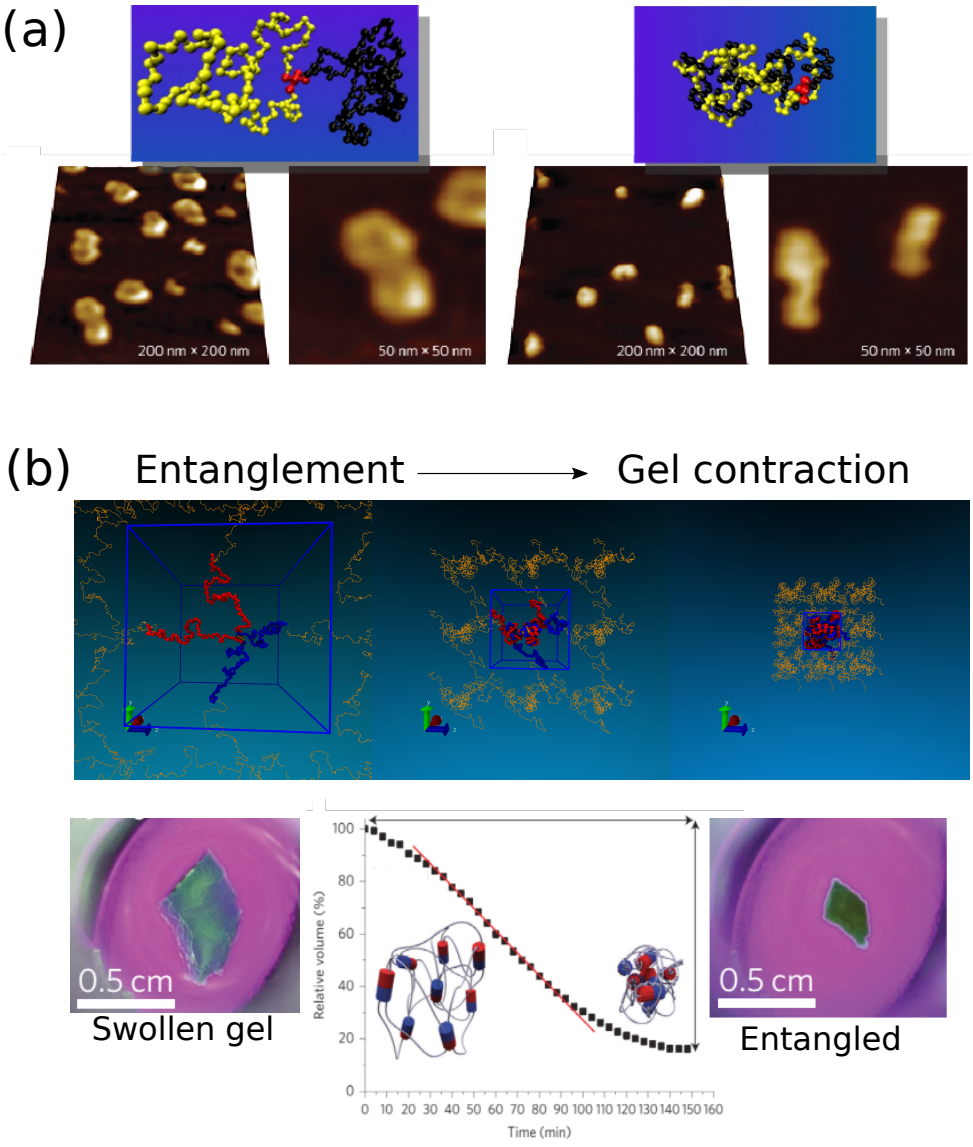

theoretically.

Unfortunately, these previously developed theories do not quite work out for a tanglotron device and a new theory had to be built for it from scratch. The reason is that the active (motor) generated torque, usually exceeds the thermal energy scale. It acts so violently on the polymer chains that the basic assumptions of classical entanglement theory become invalid. One could say that tanglotronics deals with extreme forms of entanglement that are out of bounds of the existing models.

To see why this makes a difference, consider the basic idea from classical polymer entanglement theory: a single entanglement costs some small amount energy of the order of $\sim k_B T$. If our active motor device is powerful enough to inject one , it can also inject two, ... and eventually infinitely many entanglements. But of course a pair of finite polymer chains cannot support infinitely many entanglements. Thus, an upper storage capacity of the sister chains has to be woven into any practically working theory of a tanglotron.

Another important aspect is the geometric arrangement of the polymer sister-chains. At even moderate torques, the chain configuration abruptly switches from entropic blob-like coils (as considered in classical polymer models) into a rather ordered double-helix like arrangement in the tanglotronic case. Here we see an interesting, rather general motif behind topological interactions in real materials: If topology is driven to its extremes (i.e. the density of entanglements large) it "condenses" and reemerges as pure geometry. This makes the treatment of tanglotron gels different but also much simpler than one would naively anticipate.

Let us consider a minimalistic model in a computer simulated tanglotron gel, like in Fig. 2.3, consisting of many reticulated motors interconnected with polymer chains. When each motor generates a torque M, it pairwise entangles the connected chains and densifies them into a compact helical braided structure.

How densely do the chains pack inside of these braids? How many entanglements do they contain? To mathematically approach the answers, one can write down the two basic, antagonistic interactions in the system.

First, there is an excluded volume interaction between the monomers forbidding the monomers at positions x_i to interpenetrate. It can be formally represented as a hard core potential with $V_{hc}(x_1, x_2) = 0$ for $|x_i - x_j| > b$ and $V_{hc}(x_i, x_j) = \infty$ for $|x_1 - x_2| \leq b$.

Second, the motor torque M couples to the number of mutual entanglements that the sister-chains entrap.

The latter can be expressed in terms of the sister-chains' configurations in terms and their *Gaussian linking* number:

$$Lk\left(\{x_i\}, \{x_j\}\right) = \sum_i \sum_j \frac{(x_i - x_j)}{|x_i - x_j|^3} (x_{i+1} - x_i) \times (x_{j+1} - x_j) \tag{2.1}$$

This is the discretized version of the Gaussian linking number integral for two continuum curves. It is a remarkable 4-body functional of the two n-

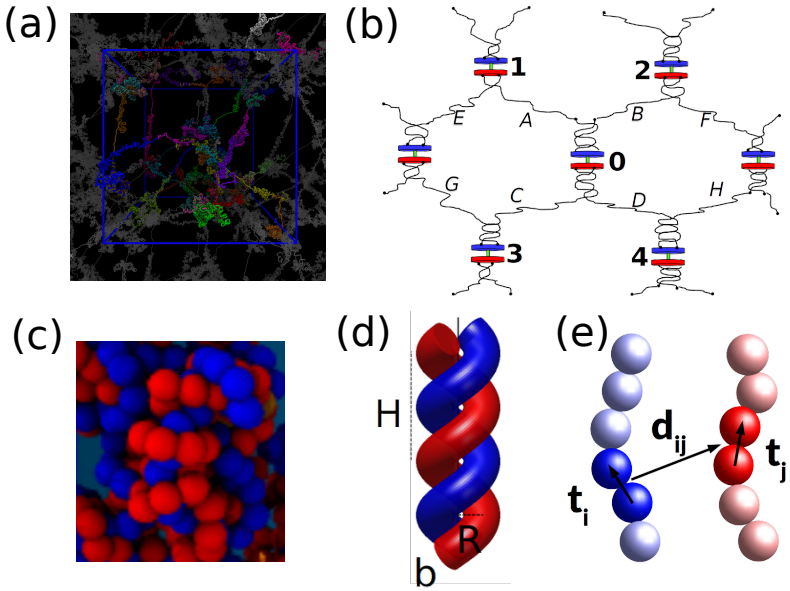

Figure 2.3: Tanglotron gels in silico and elements of its theory. a) Simulation of the entanglement process at fixed volume. Voids are opening up due to chain collapse. b) The schematics of topological interactions between different nodes. The motors 1-4 compete with motor 0 for the available chain length of chains A-D that are absorbed in their respective braids. A failure of motors 1-4 to operate is partially compensated by absorption of chains by motor 0 in its braid. c) The compacted braid structure of two braided sister-chains (red and blue) resembles a helix. d) The regular helix picture of the sister-chain braid. e) The Gaussian linking interaction of two chains is a 4-body interaction involving tuples of neighboring dimers (links) on two chains. The interaction is distance (d_{ij}) and tangent (t_i) dependent in an irreducible way.

tuples$\{x_i\}_{i=1,..n}$ and $\{x_j\}_{j=1,..n}$of sister chain monomer coordinates. The corresponding entanglement contribution to the energy can then be written as

$$E_{ent} = -M \cdot Lk$$

The statistical mechanics, configurational properties and essentially all the physics of the system are encoded in the partition function function given by the path integral

$$Z = \int\int e^{-\beta\left(\frac{1}{2}\sum_{i\neq j} V_{hc}(x_i,x_j) - M\cdot Lk(\{x_i\},\{x_j\})\right)} D\{x_i\}\, D\{x_j\}$$

where $\beta = 1/k_BT$ and $D(...)$ denotes path integration over the variable $(...)$.

If we could somehow evaluate it directly we would know everything about the system. However the innocent looking linking number Lk is a very subtle operator making the evaluation intractable in general. Where is the entanglement actually located in Eq.2.1? Because of the many body nature of the Lk operator the entanglement is actually a bit of everywhere. It lives a delocalized life- somehow similar to a quantum particle- though not in real space, but on a subset of ordered *pair of pairs* (quadruplets) of sister chain monomers as Eq.2.1 says.

But fortunately, in our limit $M \gtrsim 1k_BT$ where (statistically) ordered braids form we can simplify the problem. In this limit we can assume a helical reference state of the braid and we can expand any fluctuation around it as a perturbation. The path integral becomes "local" and factorizes , in the sense that all particles behave similarly and group together in small, well defined groups (ordered quadruplets). This line of thinking, developed in [41] works extremely well, as seen in comparisons with simulations and leads to rather simple results. For instance the linking number density (per N monomers in one sister chain) is given by

$$\frac{\langle Lk(M)\rangle}{N} = \gamma - \frac{k_BT}{\pi M} \tag{2.2}$$

where $\gamma \approx 0.3$ is a geometric constant resulting from the dense packing condition of the sister chains. The volume fraction of a tanglotron gel can also be calculated for large torques

$$\langle\rho\rangle \approx c_0 - c_1\frac{k_BT}{M} \tag{2.3}$$

with $c_0 \simeq c_1 \simeq 1$ dimensionless numerical constants of order unity.

We see that the gel is rapidly getting denser with M increasing beyond the thermal scale. Under increasing torques, i.e. for larger entanglement numbers, the two chains ,having a fixed length, can only have small spacial excursions away from their central axis and thus take less and less volume.

These asymptotic theoretical results for the linking number and density are corroborated by equilibrium simulations. And still, it seems somehow surprising that tanglotron gels as described here, behave as equilibrium objects, in

the sense that the active motor merely acts as a chemical potential on the entanglements. The reason is intuitive. The motors and the chains eventually reach a stress balance in which the motors cannot turn any more as they are prevented by the diverging free energy of the chains. In this stress balance state, the motors will in practice still dissipate energy , but the whole system can still be approximately, formally described by a thermodynamic free energy. The approximation lies in neglecting the local heating of the solvent by motors operation.

A truly non-equilibrium development of the tanlotron idea, called the tangloplex, is to make the chains bind to the motor only transiently. In such a system ,that is in one instance outlined in the perspectives section (in form of the "DNA HYPER-drive"), the dynamics and dissipative processes in the chains and the motors become crucial. The "tangloplex" development opens the door towards even richer active and dynamically responsive materials.

As often true in life: in order to get somewhere we need to let go. This is even more true for the pending tanglotron to tangloplex evolution and the possibility of unbinding of the polymer chains. Still, the modest quasi-equilibrium tanglotoron gel materials fabricated so far have quite some appeal , at least as a starting point for polymer based, topological nano-technology that shall nucleate around it.

Chapter 3

Animotion: Hydrodynamic Modes in Solids and the "Wheel Within"

In this part we describe a surprising geometric paradigm that liberates soft machines from their dependence on the wheel and axle by internalizing active rotation within the material. The "embedded wheel" motif allows us to transform many stimuli responsive materials into self-organized, continuously morphing, single-piece engines. Illustrating the concept, we show how common elastic fibers, including rubber, plastic and even spaghetti can be converted into rotary motors and self-propellers when driven out of equilibrium.

3.1 What are Animas?

A scientist from another universe discovers that his butter bread always falls onto its butter side. Remembering that his cat always falls on its legs, he comes up with a brilliant idea: He tapes the peanut-butter bread onto the back of the cat and generates an engine that lights up his universe and solves all its energy problems. Or so it goes in the classic buttered-cat paradox [143]. The system consisting of the cat and the butter-bread is apparently frustrated by construction and driven by the antagonism of its two sub-components. The only possibility it has - at least in the universes where cats and breads always fall in the same way - is to turn. This chapter is about mechanical peanut-butter-bread-cat analogues in our own world. It is also about various forms of frustration and how they give rise to continuous motion in dissipative, driven materials. For the fainthearted reader, discouraged by the prospect of facing frustration let it be said that that motion and frustration are inseparable. In fact, all natural shape and motion are borne by frustration. In the realm of physical materials, frustration denotes the inability of a system as a whole to

reach a stress-free equilibrium, in any state, at any time, in the mechanical or in the thermodynamic sense. In the following we will develop the concept of animas - mechanically frustrated active objects, that structurally encode their own motion. We will see that animas are active objects, similar to classical (macroscopic and molecular) motors, that utilize and dissipate energy in order to move in a continuous manner. Like the butter-bread-cat they give us the intuitive look and feel of an impossible object. Yet they are real, easy to make and understand.

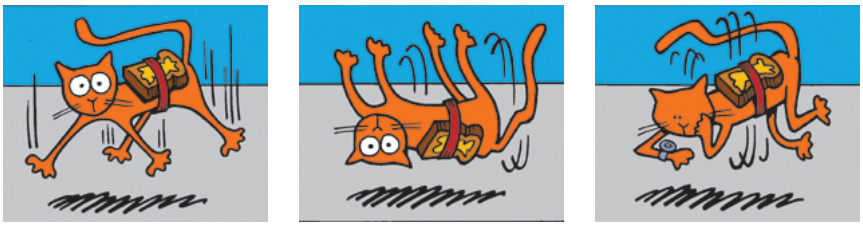

Figure 3.1: Cat and butter bread system: Cat falls on its lags. Bread on its butter side. Together they can only perpetually spin.

The prototypical example of a continuous motion-encoding object is the wheel and axle system. Once the wheel is tightly fitted onto the axle, it exhibits a natural mode of motion - its rotation around the axle. Here we will consider elastic material gadgets and machines reminiscent of the wheel, that however consist of only a *single component* and despite their simplicity display a continuous cyclic motion.

The general idea behind is to generate and then actively drive cyclic continuum zero-modes in elastic objects with internally trapped mechanical prestrains. It is well known to condensed matter physicists and formalized in the "hydrodynamic Goldstone theorem"[149] that whenever a continuous symmetry of a system is broken, there is a "symmetry restoring" deformation that can be applied to the object leaving its energy unchanged. For the Möbius tape this motion corresponds to sliding the oppositely curved regions uniformly along the length. It is somehow less known, and often overlooked in this respect, that frustrated elastic objects with hydrodynamic modes are rather common around us: from wrinkles in excess angle cones, over ribbons, to edge stressed sheets, see Fig. 3.2.

In Nature we often find zero energy modes on the micro scale, as evidenced by the universal joint reshaping of the bacterial flagellum hook[144], the wobbling motion microtubules[46] or the propulsion of left-right-handed kinks along the contractile sheet of the bacterium spiroplasma [145]. Some of these zero energy modes can even become actively driven in a directed manner by a non-equilibrium processes. Such motile or 'animated' zero elastic energy modes we will in the following pictorially call the **"animodes"**. An elastic object with an actively moving animode we might call an **anima** and the corresponding shape and energy preserving continuous deformation resulting from the action

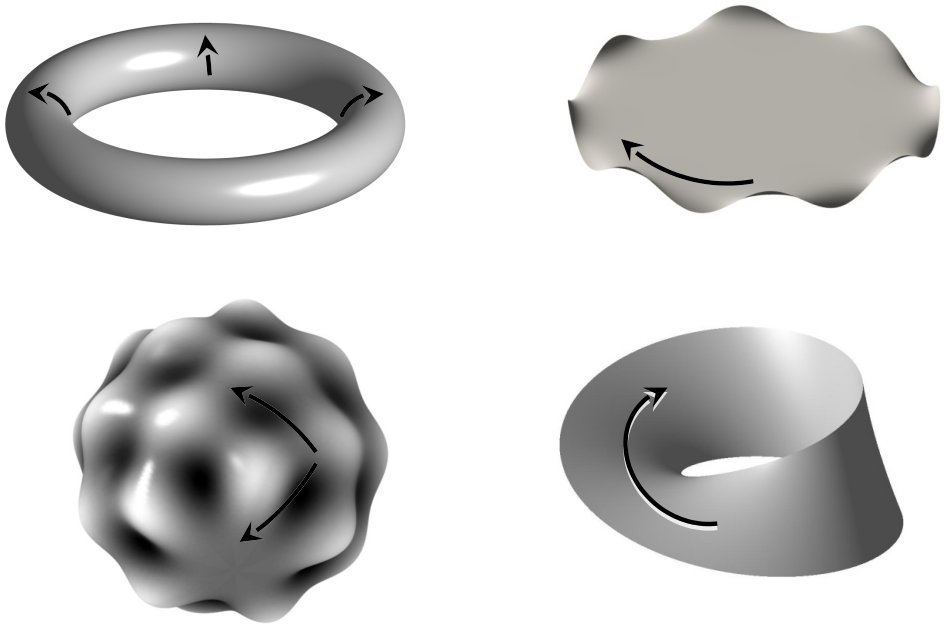

Figure 3.2: Various prestressed elastic objects exhibiting one or several zero elastic energy modes (ZEEMs). When driven out of equilibrium by an energy flux generating dynamic frustrations these objects turn into embedded "animated material" motors (animas).

of the animode we will in the following simply call **animotion**. First working examples of animas undergoing active animotion in toroidal geometries were demonstrated by us recently in [146] and consisted of a fiber closed in a circular loop. In that case the animode consists of a spontaneous, thermally driven, axial rotation of the fiber around its centerline .

3.2 Examples

Animas are not an abstract concept and are in fact rather easy to make if you know how. Animotion is so natural that it happens spontaneously in an emergent, self-organized manner. In this spirit, let us start out with some examples.

Did you ever wonder why initially straight sausages bend while being baked on the pan? At first sight, it looks like a transient thermo-elastic phenomenon, something possibly worth investigating.

A more exciting experiment (accessible for vegetarians among us as well): Take a piece of dry (uncooked) spaghetti and place it onto a flat, hot plate or a pan. You will be stunned by the observation: It rolls across the surface! This "motorization of spaghetti" is a mundane manifestation of the more general phenomenon of self-organized animotion. It also forms the basis for what we call the fiberdrive motor[146] (see also the attached manuscript).

Animotion is conceptually far more general than the spinning sausage and spaghetti which are merely its simplest practically working realization.

Another prototypical anima example is that of an intrinsically straight elastic rod closed into a loop. Placing a nylon ring onto a hot plate of a about 160-180 C, after a short warm up of about a second the ring starts to turn [1], see Fig 3.2. Note, that it does not rigidly "rotate" in a classical sense. What you observe is not rotation , it is real animotion. Note also that it has a definite directionality for any given material. For nylon and PVDF fibers, the upper portion of the ring fiber , as seen from above, moves to the outside. If you are slightly more skilled, and can handle PDMS rubber in your lab it is advisable to perform the same experiment with the rubber (curing it in a 0.5-1 mm capillary tube). What you observe is that the rubber ring turns now the opposite way with respect to the nylon ring. The reason why the ring turns is explained in sections below (and the attached manuscript) and depends on the sign of thermal expansion coefficient.

In analogy with the spaghetti, you can perform the same experiment also with a straight open piece of nylon fiber. After placing the fiber onto a slightly hot plate[2] the fiber bends slightly and begins to rapidly "rotate" and "roll" on the surface. The fiber becomes quite agile and turns into a bidirectional motor

[1] As a material it is most advisable to use piece of nylon fishing line fiber, 0.3 to 0.8 mm in diameter (for medium size to large fishes). Then close it into a loop of some 3-5 cm radius with a piece of PVDF shrink tube or brass tube connector for fishing lines.

[2] Start with 110-130 C, then increase temperature slowly (over a minute or two) up to 180C to avoid to rapid deformations which might sometimes destroy the sample.

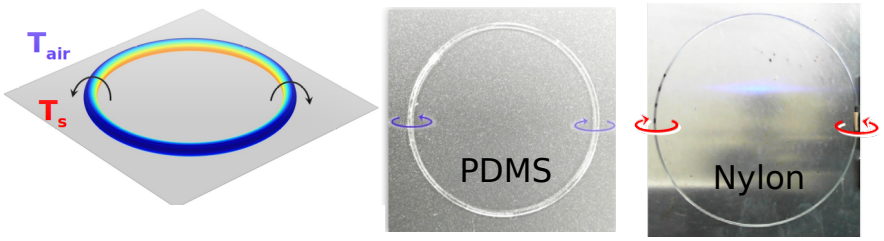

Figure 3.3: A polymer ring on a hot plate. Right panel : PDMS rubber ring turns outside-in (as seen from top) on a hot Teflon pan with a typical frequency of 1Hz. Nylon rings turn in the opposite direction (inside-out).

that can switch direction when hindered to move in one direction. You might want to confine it with two parallel obstacles (e.g. microscopy glass slides) to prevent it from falling down from the plate and to enjoy the spectacle for longer. Again , as in the case of the anima ring , the open fiber is not actually rotating and rolling , but rather constantly reshaping in its own reference frame (note the slight curvature it displays). It performs animotion again, but this time the animode is not imposed by geometry as for the ring but rather emerges through a self-induced-buckling on the plate. As mentioned, you can also perform the experiment with a piece of spaghetti , but by its very nature the spaghetti will eventually prefer to cook and seize to move (unlike the very durable nylon fibers). Nevertheless , with spaghetti you can make another remarkable observation. After moving on the plate for some seconds you can place it on a room temperature cold (˜20 C) glass or metal surface. The hot spaghetti now moves even more vigorously, till it eventually thermalizes with the plate (and the room). It is also notable and inherent to the phenomenon that on the cold surface the spaghetti will invert its movement direction with respect to its the curvature (normal vector) direction.

Active animotion is rather elegant and easy to achieve for fibers but interestingly is not restricted to fibers only. Thin sheets can display an actively driven animode as well. The probably simplest example is a rolling hollow , photoelastic cylinder excited by a light source pointed at an inclined angle [147], see Fig. 3.2. Similar design can be achieved by a thermoelastic sheet on a hot plate. In this case , the anima has to break the symmetry and structurally polarize by a first tumbling event. In both cases, these simple animas are marginally stable , in the sense that has only a single, straight contact line with the substrate. Their operation, stemming from the small weight imbalance between the, light facing, bulged and more round part, requires gravity for its operation. It can consequently develop only rather minor forces that scale with (a small fraction of) their gravity force.

A more elaborate version of a sheet anima is that of a three-fold symmetric "C_3" Möbius tape (linking number 3/2 instead of the usual 1/2). Placing such an object on a hot plate generates directed animotion , that depending on the

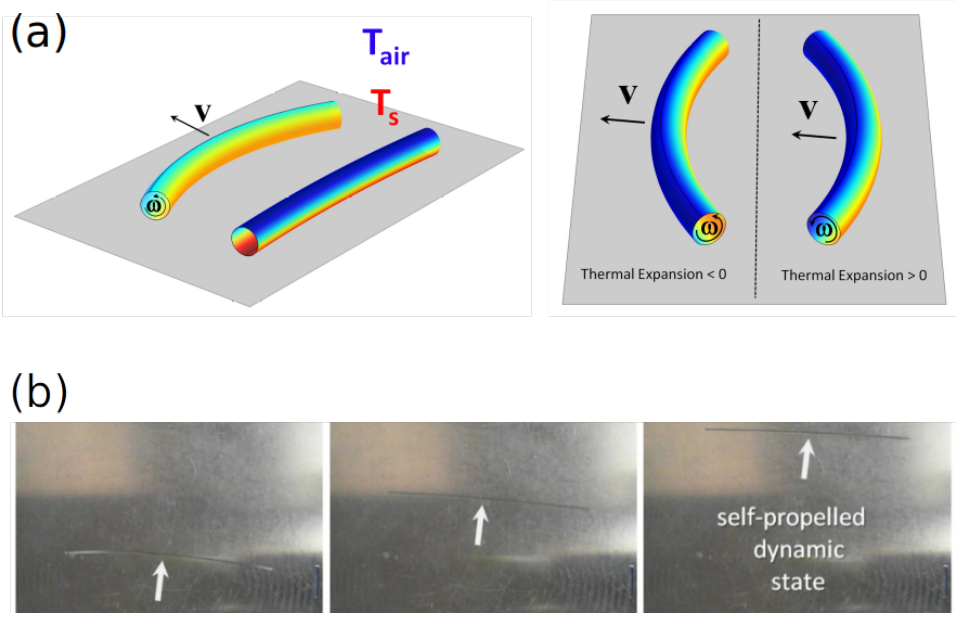

Figure 3.4: a) Fiber animas roll on hot plates. The direction of "rolling" animotion depends on the material properties. b) For nylon the rolling is to the "outside" of the formed arc.

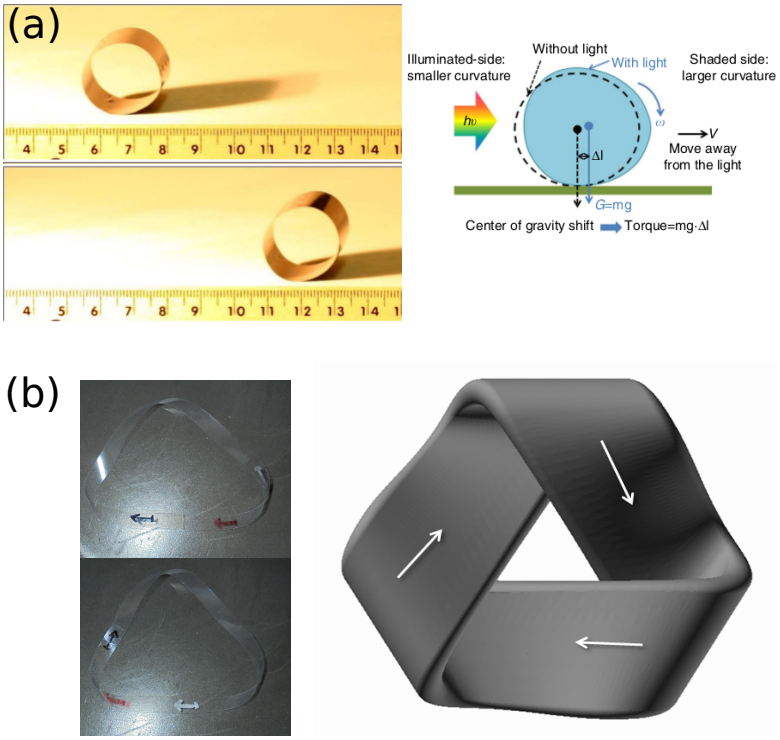

Figure 3.5: Sheet animas: a) A light responsive cylindrical sheet illuminated from the left. b) A plastic thermo responsive "C_3-Möbius strip" heated from from bottom undergoes animotion.

material can go one or the other way.

3.3 Principles of Animotion

After our excursion through examples it should be clear that we are surrounded by animotion. Here we disseminate the basic geometric and physical ingredients for active animotion in elasto-responsive systems: **static** and **dynamic frustration**.

3.3.1 Static Frustration and Zero Modes

For an continuum elastic object to display a zero elastic energy mode (**ZEEM**) ,different from a trivial rotation, it must store internal stresses that lead to symmetry breaking. That is, the object should display built-in mechanical frustration that we will refer to as built-in or static frustration. For the anima ring or the C_3-Möbius sheet anima from the previous section, the static frustration

is topologically frozen into the sample- by the constraint of closure. This is certainly the simplest way to introduce prestrain and in turn symmetry breaking of an initially symmetric and unstressed sample (straight filament and flat sheet). However , one can think of more subtle and fine-tuned, non-topological methods of introducing arbitrary prestrains. This can be accomplished by permanently shrinking or swelling different portions of the object, like for instance in an edge crumpled disk. In this case a swollen perimeter leads to disk buckling and the emergence of a zero elastic energy mode.

3.3.2 Dynamic Frustration

To initiate active motion of the object along the ZEEM we require a source of energy, more accurately, a flux , to drive the system out of thermodynamic equilibrium. The term flux , can stand for a heat flux (from a hot surface to the cold air), a flux of humidity (water or other solvents through air), or flux of ions, or even flux of photons from a light source. If the direction of the flux with respect to the elastic object and the response of the object to the flux-induced-stimulus meets certain symmetry conditions the object starts to move continuously.

3.3.3 Two Types of Animotion

Depending on how the two types of frustrations emerge, one can distinguish two types of animas. For type 1 animas the static frustration is there first , before the dynamic frustration, and together with the drive gives rise to the dynamic frustration. The zero eigenvalue of the ZEEM, that is always present at first, becomes now purely imaginary, the ZEEM turns into an animode and the object performs animotion. A typical example here is the toroidal fiberdrive. It displays a zero mode even before the drive sets it.

In type 1 animas the motion onset occurs in a continuous fashion once the drive can overcome the dissipation. In case 2, initially there is no static frustration , but it only co-emerges with the dynamic frustration once the drive sets in. A typical example is the linear fiberdrive. In contrast type 1, in a type 2 anima the system needs to buckle first and break the symmetry. The animode emerges by spontaneous symmetry breaking without originating from a ZEEM. This happens only after crossing a certain threshold of driving power and typically with a rapid, discontinuous velocity of motion at the onset. A central characteristics distinguishing type 1 and type 2 animas is that the former (type 1) is a unidirectional engine, while the latter (type 2) is a bidirectional one , that can flip its direction typically randomly after being stalled. In general, from practical point of view, the type 2, bidirectional animas will be simpler to build, even on smaller scales, as their prestrain emerges spontaneously. However their bidirectional nature will render them far less useful as an engine. The unidirectional, type 2, animas will require some more assembly effort (like e.g. fiber circularization) but are much more naturally suited as robust engines.

3.3.4 Interactions with Stimuli

To become active , the material has to be "smart" and respond to an external driving stimulus. The stimulus, that we for simplicity assume to be a scalar quantity T can be anything from temperature, over a chemical's concentration in the solution or the intensity of light. In the simplest case the stimulus can induce an isotropic prestrain (eigenstrain, cf. [152]) proportional to the driving field: $\varepsilon_{ii} = \alpha T$ where α is the coupling coefficient and ε_{ij} the elastic strain tensor [3]. An important requirement for animotion is that the scalar stimulus field T must be out of equilibrium. That means in particular that it displays gradients and directional fluxes along these gradients. If we think of T as temperature of a hot plate in cold air, there will be a heat flux opposing the stimulus' gradient ∇T. In the simplest case, of a uniformly heated plate, the stimulus gradient is uniform within the plane and points everywhere along the plane's normal - in the z-direction. In the case of directional parallel light stimulation , the gradients in the light intensity field will appear through the absorption within the material itself. The directly illuminated side of the semitransparent or opaque object will get more photons, absorb them so that less photons arrive on its shadowy side.

When acted upon the stimulus gradient, different layers of material sample will respond with different stains at different depths. That is, a stimulus gradient leads to a strain gradient along the same direction. It is easy to see that a material with a negative stimulus coupling coefficient $\alpha<0$ (like e.g. nylon upon heating) will curve in the direction opposing the flux and form a con**cave** bridge or "cave". Similarly , a positive stimulus coupling coefficient $\alpha>0$ (like heated rubber) will lead to a bend in the direction of the flux and form a con**vex** valley, here simply called a "vex". So , for any specific material every section of it will tend to "cave" or "vex" towards or away from the gradient. If however the closure constraint forbids or constrains such deformations, they will project in another direction and this frustrated projection initiates animotion.

The geometry and active mechanics of vexing or caving contact points in intricate geometries can become really complicated. This is particularly true for 2d sheets (cf. the C_3Möbius tape), that display an intrinsic coupling of Gaussian curvature with the in-plane stretching. Fortunately, to understand the emergence of the animode we have a simple prototype that is still elementary enough to study - the toroidal animotion of the "fiberdrive".

[3] We will focus here on this elementary, isotropic , linear coupling case. Note that many of the assumptions we made, like the isotropy of the material and material expansion, or a scalar stimulus are not really necessary and are chosen to keep it simple. Generalizations to vectorial stimuli (like the e.g. polarization vector of light) , anisotropic coupling of the material to the vectorial stimulus, as well as the stimulus affecting not only the prestrains but also the elastic moduli are possible, opening up some avenues towards vast and interesting playgrounds.

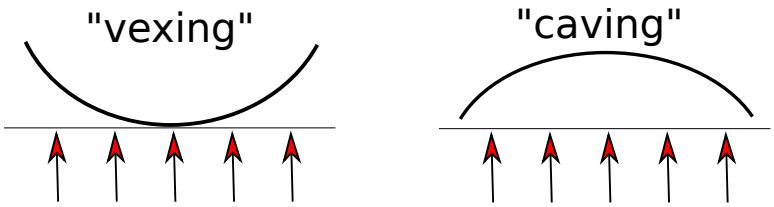

Figure 3.6: Stimulus response, vexing and caving. A material sample can react to an energy flux (red arrows) in two ways: it can become convex and bend away ("vexing") or concave, bending towards the flux ("caving").

3.4 Toroidal Animotion

In an nutshell , toridal animotion happens because the lower part of the torus contracts or extends and thus "wants" to vex or cave (depending on the material). If the material contracts (extends) upon heating, the lower portion of the torus migrates towards the inside (outside) of the torus. That sets the direction of animotion. Physically, this the simple (and extremely robust) essence of toroidal animotion. To understand it deeper in the following sections and in an appendix (at the end) I develop the backbone of a future theory and a classification of different types of animas. The theoretically less inclined reader can skip the starred (*) chapters down to.

3.4.1 The Toroidal ZEEM

Consider a torus, made out of a stimulus responsive, isotropic and linearly elastic material rod (think of rubber or nylon rod) closed in a circular loop. The stimulus, here assumed to be temperature T, gives rise to a temperature profile within the material and has a flux ∇T. The latter we assume here for simplicity to be symmetric around the torus symmetry axis (the z-axis), i.e. all torus sections behave in same manner. Consider a single section of the torus and a coordinate system attached to the material. Along the two embedded coordinate axes ,call them $\mathbf{e_1}$ and $\mathbf{e_2}$, we will have a temperature profile that in first approximation we assume to be a linear gradient. The two corresponding co-moving gradient components, projected onto the co-moving axes, we denote with $\theta_1 = \mathbf{e_1} \cdot \nabla \mathrm{T}$ and $\theta_2 = \mathbf{e_2} \cdot \nabla \mathrm{T}$. The internal coordinate frame can dynamically reorient with respect to the outer, lab-fixed frame , $\mathbf{e_x}$ and $\mathbf{e_z}$ by a uniform "rotation" of all cross-sections by an angle $\Phi(t)$ (evolving with time t) like

$$\mathbf{e_1} = \cos(\Phi)\mathbf{e_x} + \sin(\Phi)\mathbf{e_z}$$
$$\mathbf{e}_2 = -\sin(\Phi)\mathbf{e_x} + \cos(\Phi)\mathbf{e_z}$$

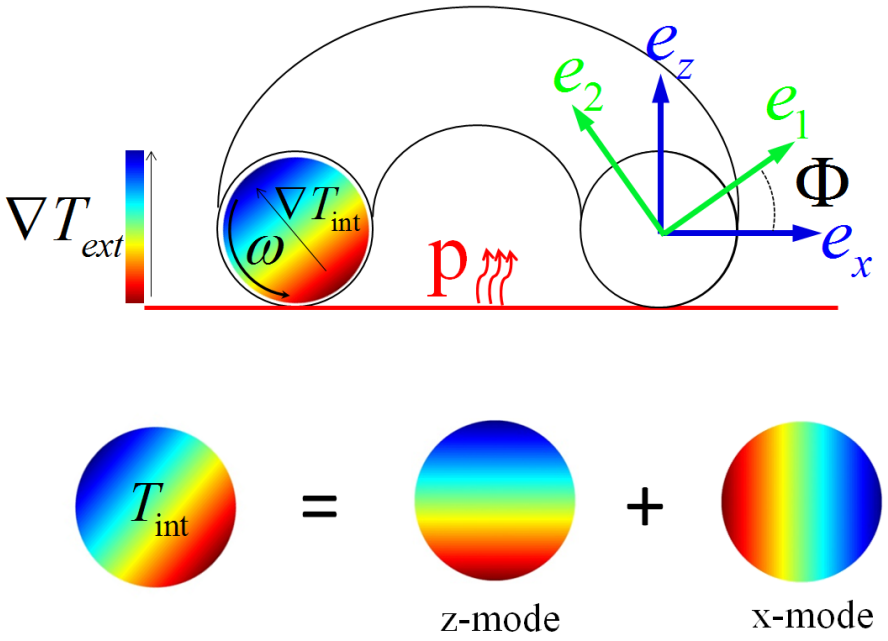

Figure 3.7: The geometry of toroidal animotion. The internal temperature profile T_{int} of each cross-section is decomposed in two modes. The thermal **z-mode** is pumped by the heat flux p normal to the substrate (represented by the red horizontal line). The **x-mode** emerges from the z-mode by frame rotation (animotion) with the angle Φ.

Note that this $\Phi-$"rotation" of the cross-section is *not* a rigid body motion of the whole object. It is rather a continuous deformation and reorientation of the whole torus along its ZEEM. Parametrising the torus $X_{tor} = (x, y, z)$ with two angles θ, φ and the distance $\rho \leq r$

$$\begin{aligned} x(\rho, \theta, \varphi) &= (R + \rho\cos\theta)\cos\varphi \\ y(\rho, \theta, \varphi) &= (R + \rho\cos\theta)\sin\varphi \\ z(\rho, \theta, \varphi) &= \rho\sin\theta \end{aligned}$$

the elastic displacement field $\overrightarrow{u}$ of the toroidal ZEEM can be written as

$$\overrightarrow{u}_{ZEEM}(\rho, \theta, \varphi) = \frac{\partial \overrightarrow{X}_{tor}(\rho, \theta, \varphi + \epsilon\Phi)}{\partial\Phi} \tag{3.1}$$

where $\epsilon\Phi$ stands for an infinitesimally small motion along the φ coordinate. This displacement field can be written down more explicitly , but it is already clear that this is no naive, simple rotation. The toroidal ZEEM a new beast in town.

3.4.2 Frustration and Emergence of Torque (*)

The body-fixed temperature gradients θ_i naturally give rise to eigen-strain gradients $\nabla\varepsilon^e_{zz}$ along the long toroid axis and intrinsic eigen-curvatures

$$\kappa^e_i = e_i \cdot \nabla\varepsilon^e_{zz} = \alpha e_i \cdot \nabla T$$

where α is the thermal expansion coefficient (with units K^{-1}). These internal frame (preferred) "eigen" curvatures κ^e_1, κ^e_2, relate to the external frame eigen-curvatures κ^e_x, κ^e_z in the same way that the two coordinate systems transform :

$$\begin{aligned} \kappa^{\mathrm{e}}_1 &= cos(\Phi)\kappa^{\mathrm{e}}_{\mathrm{x}} + sin(\Phi)\kappa^e_{\mathrm{z}} \\ \kappa^e_2 &= -\sin(\Phi)\kappa^{\mathrm{e}}_{\mathrm{x}} + \cos(\Phi)\kappa^{\mathrm{e}}_{\mathrm{z}} \end{aligned} \tag{3.2}$$

with the inverse transform:

$$\begin{aligned} \kappa^{\mathrm{e}}_{\mathrm{x}} &= \cos(\Phi)\kappa^{\mathrm{e}}_1 - \sin(\Phi)\kappa^{\mathrm{e}}_2 \\ \kappa^e_{\mathrm{z}} &= \sin(\Phi)\kappa^{\mathrm{e}}_1 + \cos(\Phi)\kappa^{\mathrm{e}}_2 \end{aligned} \tag{3.3}$$

The upper index e in κ^e_1, κ^e_2 and κ^e_x, κ^e_z indicates that we are dealing with the *preferred* eigen-curvatures that the rod *would* assume if it was free to reorient in space. However, the rod is not free. It is closed in a torus, lying in a plane with normal $\mathbf{e_z}$. This imposes a strict condition on the actually *assumed* curvature (written without index) in the external frame. This actual curvature is given by

$$\kappa_x = 1/R \tag{3.4}$$

$$\kappa_z = 0 \tag{3.5}$$

where R is the (large axis) radius of curvature of the torus. The mismatch between the preferred value of a variable κ_i and its actual, assumed value, i.e. the quatity $(\kappa_i - \kappa_i^e)$, can also be called the "*frustration*". It has a corresponding "frustration energy" given by $E_i = \frac{K}{2}(\kappa_i - \kappa_i^e)^2$ with $K = BL$ an elastic constant, given by the bending stiffness B of the torus of contour length $L = 2\pi R$. Having two orthogonal modes, the total frustration energy is the sum of the mode energies in both of the coordinate systems:

$$E = \frac{K}{2}\left[(\kappa_1 - \kappa_1^e)^2 + (\kappa_2 - \kappa_2^e)^2\right] \tag{3.6}$$

$$E = \frac{K}{2}\left[(\kappa_x - \kappa_x^e)^2 + (\kappa_z - \kappa_z^e)^2\right] \tag{3.7}$$

For given preferred material eigen-curvatures $\kappa_{1/2}^e$ and the actual, imposed curvatures $\kappa_{1/2}$, Eq. 3.5, inverting the transformation in Eq. 3.2 and inserting in Eq. the energy simplifies

$$2E(\Phi)/K = (\kappa_1^e)^2 + (\kappa_2^e)^2 + \frac{1}{R^2} - \frac{2}{R}\left(\kappa_1^e \cos\Phi - \kappa_2^e \sin\Phi\right) \tag{3.8}$$

For vanishing eigen-curvatures $\kappa_1^e = \kappa_2^e = 0$ (i.e. if there is no heat flux) the energy is independent of Φ as expected from toroid's ZEEM (that is parametrized by Φ). However with non-vanishing eigencurvatures κ_i^e (e.g. when we heat from below) the ZEEM is "broken" and the toroid assumes a fixed, unique Φ in its equilibrium state. The system would also stay in that (quasi) equilibrium if it was not constantly driven and dissipating.

3.4.3 Dynamics (*)

The mechanical dynamics of the toroid anima with non-vanishing κ_i^e results from a balance of torques acting on the variable Φ. On the one side there is the elastic torque $M = -\partial E/\partial\Phi$ resulting from the energy (Eq. 3.8)

$$M_{el}\left(\Phi\right) = \frac{K}{R}\left(\kappa_1^e \sin\Phi + \kappa_2^e \cos\Phi\right) \tag{3.9}$$

In addition to the elastic torque, when the toroid is moving there is typically also a dissipative torque

$$M_{diss} = \xi\frac{d\Phi}{dt} + C\text{sign}(\dot{\Phi}) \tag{3.10}$$

One can think of the first term as as an effective, internal or external, Stokes-like friction with a friction constantξ. The second, slightly inelegant but in practice rather important term is the solid, coulomb type friction. It is independent of the velocity magnitude but depends on the direction of motion , signified by the sign of $\frac{d\Phi}{dt}$ term. This dry friction typically acts at the interface between the object and the substrate. Furthermore, most glassy, plastic materials, like nylon, also exhibit an internal dry friction at low velocities.

For the sake of simplicity we omit here the dry friction term and balancing the two torques we get the dynamic equation

$$\frac{d\Phi}{dt} = \tau_e^{-1}\left(k_1 \sin\Phi + k_2 \cos\Phi\right) \tag{3.11}$$

with $k_{1/2} = R\kappa^e_{1/2}$ the eigen-curvatures in non-dimensional form and $\tau_e = R^2\xi/K = \frac{L\xi}{4\pi^2 B}$ a characteristic "elasto - hydrodynamic" timescale governing the relaxation to the mechanical equilibrium.

When we switch-on the active drive, like heating the torus from the bottom, the the internal eigen-curvature modes $k_{1/2}$ themselves become dynamic. With an upwards (heat) energy flux, the two modes increase with a "pumping rate" $p \propto \alpha\Delta T$ according to their current projections on the z-direction (direction of heat flux). Counterbalancing the energy influx, the $k_{1/2}$ modes also have to spontaneously decay by giving off heat to their environment. This happens with a rate $rk_{1/2}$ proportional to their own magnitude. Taken together, it is intuitive to asume (and can be formally shown by solving diffusion-advection type equations, see [146]) that the modes evolve as

$$\frac{dk_1}{dt} = p\sin\Phi - rk_1 \tag{3.12}$$

$$\frac{dk_2}{dt} = p\cos\Phi - rk_2 \tag{3.13}$$

3.4.4 Type 1 Animotion (*)

The system of 3 equations 3.11-3.13 govern the dynamics of the intrinsic curvature in the co-moving frame. To solve them , we can rewrite them in the external, lab-fixed frame, with the corresponding scaled eigen-curvatures $k_{z/x} = R\kappa^0_{z/x}$. Defining the angular frequency $\omega = \frac{d\Phi}{dt}$ from Eq.3.10 the Eqs. 3.11-3.13 simplify to

$$\omega = \tau_e^{-1}k_z \tag{3.14}$$

$$\frac{dk_x}{dt} = -rk_x - \omega k_z \tag{3.15}$$

$$\frac{dk_z}{dt} = p - rk_z + \omega k_x \tag{3.16}$$

The first equation originates from the mechanical torque balance, while the second and third are "thermodynamic" (diffusion-advection like) in nature. Taken all three dynamic equations , we have an interesting steady state obtained by setting $dk_{x,y}/dt = 0$:

$$\begin{aligned} k_z &= \tau_e\omega, \quad k_x = -\tau_e r^{-1}\omega^2 \\ p &= r\tau_e\omega + r^{-1}\tau_e\omega^3 \end{aligned} \tag{3.17}$$

From the last equation we see that (in absence of dry friction) there is motion for arbitrary small drive p. Close to the onset , at small drive $p \to 0$, where ω is small as well, we have then simply

$$\omega(p) \approx \frac{p}{r\tau_e} \tag{3.18}$$

Inverting the drive $p \to -p$ leads also to an inversion of animotion direction i.e. angular velocity switches sign, $\omega \to -\omega$. This is a typical behavior for *type 1 animas*. Their direction of motion is set by the geometry and (in the case of negligible dry friction ,as assumed here), the motion is present for any arbitrary small magnitude of the stimulus p.

3.4.5 Type 2 Animotion (*)

What happens if we do not impose the symmetry of stimulus flux , to be from the bottom , but let say radially from the inside to the outside of the toroid? Such an arrangement can for instance be reached by inserting a hot cylinder in the inner "hole" of the torus, radiating the heat flux from the inside to the outside. In such a case the mechanical equation 3.11 stays unchanged and only the thermo-elastic equations 3.12 and 3.13 become modified by the change of flux orientation to

$$\frac{dk_1}{dt} = p\cos\Phi - rk_1 \tag{3.19}$$

$$\frac{dk_2}{dt} = -\ p\sin\Phi - rk_2 \tag{3.20}$$

Transforming again from the body-fixed to the lab-fixed frame we obtain

$$\frac{dk_x}{dt} = p - rk_x - \omega k_z \tag{3.21}$$

$$\frac{dk_z}{dt} = -rk_z + \omega k_x \tag{3.22}$$

where ω still obeys 3.14. The new equations 3.21,3.22 are very similar to 3.15,3.16 , with roles of the two modes flipped. However in combination with 3.14 the steady state now becomes

$$\omega\left(p - r^2\tau_e - \tau_e\omega^2\right) = 0 \tag{3.23}$$

The system now behaves dramatically different. For $p < r^2\tau_e$ the only solution is $\omega = 0$, i.e the system is static and no motion is possible. For $p_{crit} = r^2\tau_e$ it exhibits a pitchfork bifurcation, the static solution becomes unstable and **two** new stable branches,$\omega_+$and ω_-,emerge

$$\omega_\pm(p) = \pm\sqrt{p/\tau_e - r^2} \tag{3.24}$$

Therefore, beyond a critical pumping $p > p_{crit}$ (sufficiently large to overcome dissipation) the system breaks the symmetry and displays an animode in one of the two directions. This bi-directionality and the presence of a threshold are the defining characteristics of *type 2 animas*.

In our concrete, radially heated torus case, we have an interesting particularity: when we invert the sign of p we also dramatically change the dynamic behavior of the system (as p comes in first power). This, behavior which is not quite general for all type 2 animas (as we will see in next section), physically comes from the fact that when we heat from the inside of the torus and the material prefers to contract upon heating (i.e. a "caving" material) the heated part stays stably at its original position (in the middle). In this case, statically stable case, obviously no motion is observed. Only when the hot part on the inside likes to expand (i.e. when we are dealing with a "vexing" material) do we get a dynamic frustration which leads to the onset of animotion.

3.4.6 The Motile Spaghetti (*)

As we discussed in a previous chapter even a cylindrically symmetric object can become an anima if it is forced to stay in plane and driven in the z-direction. In this case the actual in-plane curvature κ_x is free to adjust to the preferred in-plane eigen-curvature κ_x^e, i.e. $\kappa_x = \kappa_x^e$. The out of plane curvature on the other hand, necessarily vanishes i.e. $\kappa_z = 0$. Together this gives rise to an elastic energy of the form

$$E = \frac{K}{2}(\kappa_z^e)^2$$

with the resulting elastic torque

$$M = -K\kappa_z^e\kappa_x^e$$

Compare these expressions to their closed toroid equivalent Eq. 3.7 where both eigen-curvatures enter and both actual curvatures are constrained.

Going through the exercise of balancing torques like in 3.93.10, dropping again the dry friction, the equations for the (scaled) eigen-curvatures in the lab-frame become

$$\omega = -\tau_e^{-1}k_z k_x \tag{3.25}$$

$$\frac{dk_x}{dt} = -rk_x - \omega k_z \tag{3.26}$$

$$\frac{dk_z}{dt} = p - rk_z + \omega k_x \tag{3.27}$$

The Eqns. 3.263.27 are of course identical[4] to Eqs. 3.153.16 as the kinematics of inducing strain in z-direction (the p term), dissipating heat (the r term) and the

[4]In absence of an intrinsic, closure imposed radius $R = L/2\pi$ the scaling of the variables k_x, k_z and the timescaleτ_e can be done by the filament's length L instead.

mode advection (the ω term). Only the torque-balance equation 3.25 deviates from its toroid counterpart 3.14 by an additional $-k_x$ term. Solving for the steady state we obtain

$$\omega \left(r\tau_e \left(r^2 + \omega^2 \right)^2 - \ p^2 r^2 \right) \quad = \quad 0 \tag{3.28}$$

The branch $\omega = 0$ is stable for sub-critical pumping $|p| < p_{crit}$ with $p_{crit} = \sqrt{r\tau_e}$. For $|p| > p_{crit}$ the $\omega = 0$ branch is unstable while two new branches

$$\omega_{\pm}(p) = \pm \sqrt{\frac{rp^2}{\tau_e} - r^2} \tag{3.29}$$

emerge. Again, with the bi-directionality and symmetry breaking involved, we are dealing with a type 2 anima. Interestingly , when we compare the kinematic relation Eq. 3.29 to the one in Eq. 3.24 from the toroidal type 2 anima case difference in the exponent of the p term stands out. In the present case , Eq. 3.29, inverting the direction of the pumping does not change the physics (p comes in the second power). Regardless if we are cooling or heating from below: upon sufficient pumping , the fiber is rotating and rolling bi-directionally in plane.

3.5 Animas as Motors

From the previous examples we have learned that there are two distinct classes of animas: those who run easily and uni-directionally (type 1) and those, bi-directional ones that need to break a symmetry to decide which way they run (type 2 animas). The distinction is not a mere mathematical subtlety. It touches upon the practical utility of the anima as motors. A device that inverts its direction upon weak opposition in its surrounding is dynamically less robust than an object that turns unidirectionally and without any threshold[5]. For the physics of the two types of animas considered as motors is referred to the Appendix, where I give the torque-velocity relation for various types of anima devices.

[5]The "without threshold" statement for type 1 animas has however to be taken with a grain of salt and is true only in absence of an external torque and in absence of dry friction. So far we have ignored dry friction which can naturally induce a threshold even in a system that does not break symmetry. Although dry friction has something of an analytical nuisance -due to its singular velocity independent nature- it is basically always present. It is often even dominant over other forms of friction on the macroscopic scale and small speeds. Not surprisingly dry friction modifies the onset of animotion, such that there is always a minimal pumping threshold that needs to overcome the constant friction force. Leaving technical details to later work one can still state, that apart from the shift of onset, animotion keeps its character regardless of particular type of friction.

3.6 Outlook

We have explored here a novel paradigm that we called animotion. When looking back at what it "really" means, it actually represents a new form of active "wheel within the material". From the examples above we have seen the practical feasibility of embedding the wheel and driving mundane polymer fibers as motors. These fibers turn into robust, one-piece motors ("fiberdrives") when driven away from equilibrium due to dynamic frustration emerging within the material. We have seen that zero elastic energy modes (ZEEMs) are truly ubiquitous in elastic material samples and generating dynamic frustration to drive them can be as easy as placing a spaghetti on a hot stove. The model that we developed above suggests that many other driving mechanisms should potentially induce animotion. In fact, the energy pumping rate p (initially represented by a heat flux) could be substituted by any flux normal to the plane. Fluxes that can couple to the material's strain, could in principle be anything from solvent, ionic/pH, electrical fluxes to optical illumination gradients that we are exploring in particular these days. The insight that we can now fully dispense with the ancient wheel and axle, utilize intrinsic ZEEMs and make them perform animotion instead, opens some exciting new perspectives on soft machines. The anima motors, made from mundane plastic, rubber and even starch call for rethinking the very meaning of a "smart material" . In fact the concept of animotion shifts the spotlight from microscopic material properties to mathematical ideas of symmetry and topology. Through them the physical material acquires a novel form of collective smartness, residing in none of its individual parts, yet globally encoded in their delicate interplay.

Considering the enormous simplicity and robustness of animotion it appears to be a likely mechanism to stumble upon by evolutionary chance. From experience we learn that rarely we can come up with something really simple and functional that Nature did not explore already. Now here is a tantalizing thought. Owing to their unusual filamentous shapes filoviruses including the marburg and ebola virus might display some form of gradient driven surface rolling motility (possibly driven by humidity or ion gradients). The hypothesis, of filovirus animotion, right or wrong, is too scary to be ignored easily and certainly requires further attention.

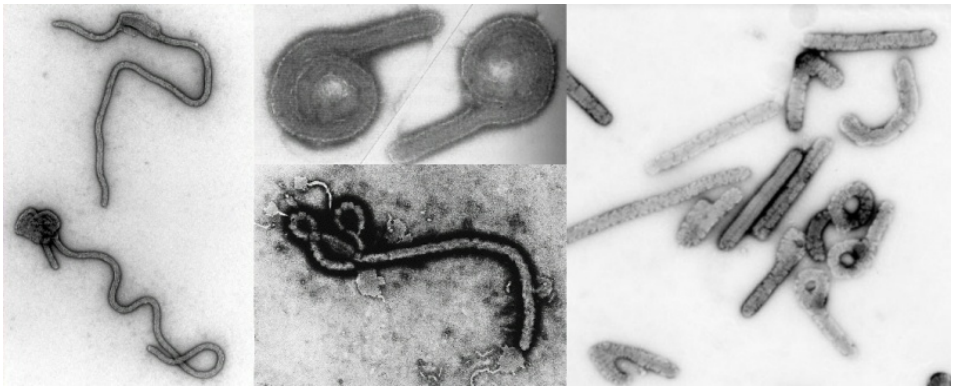

Figure 3.8: A tantalizing ramification: Ebola virus animotion and propulsion on surfaces?

Chapter 4

Projects in the Making: DNA Nanomotors, Anima Motors , Confotronic Fibers

Looking forward, there are some concepts that have crystallized out and call for further development in various directions. Among them, three really stand out and should bear fruit in future: a) concepts of confotronics and their implementation (in particular the synthetic ones yet to come), b) further generalization of the tanglotron coupling and c) practical continuum material (anima) motors. My plans for future can be subdivided in "improvements" of ideas and conceptually "new directions".

4.1 Animotion and Fiberdrives

To build truly complex continuum machines from smart materials it seems inevitable to think broader, beyond the pure material properties and reflect on material geometry and topology. In the future we will develop deeper the newly proposed paradigm -animotion - allowing us to build complex continuum machines, in particular circular motors from single pieces of smart, responsive materials. The general idea to induce and actively drive cyclic continuum zero-modes in elastic objects with internally trapped mechanical prestrains was demonstrated to be practical and conceptually sound. One example already outlined above is the closed torus operated as a motor (fiberdrive). This seems to be the first , but certainly not the only instance of such a continuously deforming object. As a second example, one can think of sheets and ribbons. Their practical utility , torque and power density will also be investigated in near future.

4.1.1 Optical Driving, Down-Scaling, First Devices

Over the past two years, we have demonstrated that the fiberdrive can be driven by a heat source. This can be seen as a proof of concept but somewhat inelegant and brute force approach. It is practically preferable to work with other sources of energy like electrical fields or light. One interesting hint that electrical fields could be utilized to operate the fiberdrive is our finding that besides nylon and silicone rubber also PVDF fibers exhibit the thermoelastic rotation (comparable to that of nylon). PVDF has several amazing properties and stands out among polymers : it is piezo, pyro- and ferro-electric. This could open the path towards electrically driving single PVDF fibers once its semi-crystalline lamelar domains have been properly poled (oriented). Another alternative and even more promising path is to embed photo-switchable azo-benzene molecules within a polymer matrix and utilize light as an energy source. Recently, in collaboration with a newly recruited chemist Amparo Ruiz and a motivated master student we have managed to synthesize the necessary material components. With quite some excitement we are looking forward to test soon the first optical fiberdrive.

It appears that when scaled down animas could play a similarly important role in micro and nano-mechanics as the wheel has played in the macroscopic machines. The favorable scaling was first demonstrated in the thermic drive case, where we found that fibers of 100 micron or less rotate with frequencies of tens of Hz. In future we will closer explore the laws and practical (engineering) limits of anima fiber down-scaling and put it to practical use, at least a a proof of concept level . In simple microfluidic channels optical versions of the fiberdrive could act as light driven rotary mixers and pumps.

4.1.2 Making of Open Anima Fibers

Another interesting project is to build open amima fibers that even in absence of drive exhibit a zero elastic energy mode (ZEEM).

There are indeed microscopic fibers that behave in that way including bacterial flagella and microtubules. The hope that we can really make such an object is based on recent theoretical considerations but also some interesting macrosopic experiments that we have performed. In them we have demonstrated that when putting tensile prestress on a cylindrical tube's outer layers (i.e. the "skin") while keeping the core of it unperturbed , there is a novel elastic instability that leads to self-buckling and the formation of a continuous ZEEM. It behaves similar to the ZEEM seen in a rod closed in a torus (cf. the fiberdrive) but without the necessity to have the two ends topologically closed (i.e. to form a complete torus). I

Through their spontaneous , zero-mode curvature , such "ZEEM fibers" could significantly improve the torque and power output of a fiberdrive device (cf. above) and more generally act as novel scalable universal joints transmitting torques "around the corner" in future soft machines. From the practical side, we will try to make a higher throughput procedure to generate larger lengths (meters) of anima fibers and think about the prospects for their industrial utility

and larger scale production.

4.2 Sythetic Confotronics and Artificial Axons

4.2.1 DNA Nanomachines I: The DNA HYPER-drive

In the tanglotron project we have utilized a form of the Feringa photo engine to generate macroscopic motion and store free energy in entanglements. Despite its beauty, the Feringa engine is rather chemically fragile, susceptible to oxidation and can be effectively only used in organic solvents, which severely limits its versatility and in particular biocompatibility. To overcome these shortcomings we plan to build a DNA rotary nano-engine, that will be fast (faster than 1 Hz) , powerful (torques of several kT) and electrically driven (voltages of few Volts). In fact the construction of such a device is currently on the way in our lab.

The basic idea for this novel motor ,that we will in following call the HYPER drive (or the Hybridization Pawl Electric Ratchet), is conceptually simple, see Fig.3.2. The DNA motor generates torques at the interface between two surfaces, one being a gold electrode and the other a plastic micro-bead. The basic structural element of the HYPER drive is a DNA cruciform (Holliday junction), here referred to as the "zipper", that acts as a translational and rotational pawl of the ratchet mechanism. The operation of the zipper rotates the two "legs" via an electric field driven branch migration process. At the same time the zipper extrudes and pulls off the "feet" sequences from the short sticker strands attached to the upper surface (the bead).

The branch migration is induced by changing the polarity of the electrode surface to which the DNA strands are chemically bonded. When the electrode is at positive potential (w.r.t. a reference electrode at infinity) the DNA is pulled towards the electrode's surface. The electrostatic interaction, that happens over the typical scale of a Debye length, leads to a branch migration of the cruciform. The cruciform reshapes such that its 2 branches parallel to the surface become extend and the 2 orthogonal ones contracted accordingly. This process leads to a combined rotation and retraction of the legs. Switching the potential to negative reverts the branch migration process, effectively pushing the DNA away from the surface while generating a rotation of opposite sign (w.r.t. the negative potential case).

Through a proper choice of signal shape of the of the electrode potential (frequency, amplitude and asymmetry) the construct becomes a rotary ratchet that can generate an effective rotation of the bead relative to the electrode surface. A full rotation happens over timescales of several branch migration cycles each one of which being in the range of 10-100 microseconds.

Once completed the HYPER drive will be the first really fast and physical field driven DNA based motor. Being fabricated out of DNA it would have a number of important and useful features. It would work in water , under close to physiological conditions . Furthermore, it would be fully compatible with and able to interface to the growing number of available nano-structures generated

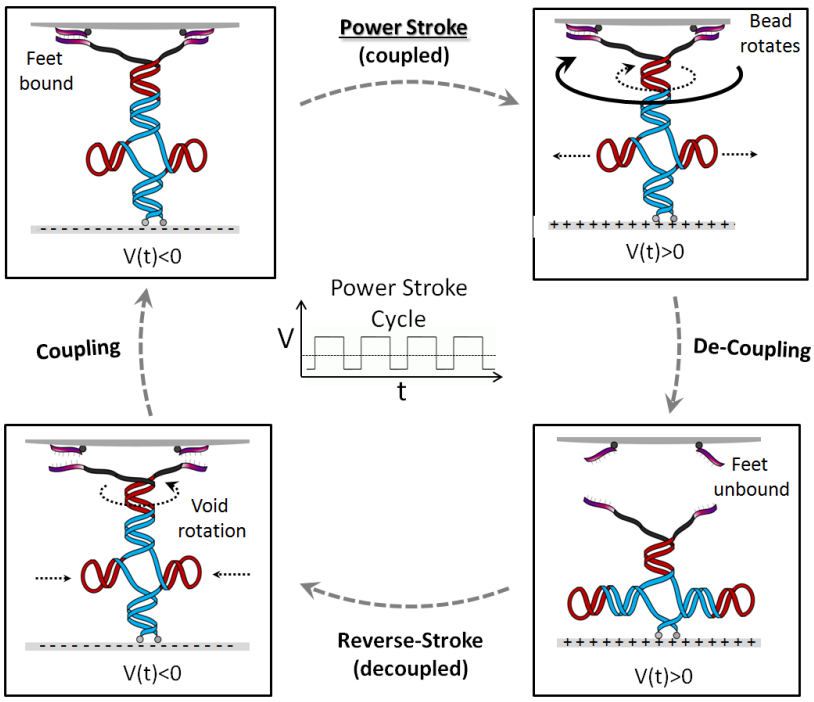

Figure 4.1: Power stroke cycle of the HYPER drive induced by periodically oscillating polarity of the gold electrode (lower surface). Based on the Brownian ratchet effect, the nano-device generates a continuous rotation of the upper surface (DNA-oligo covered bead) with respect to the electrode.

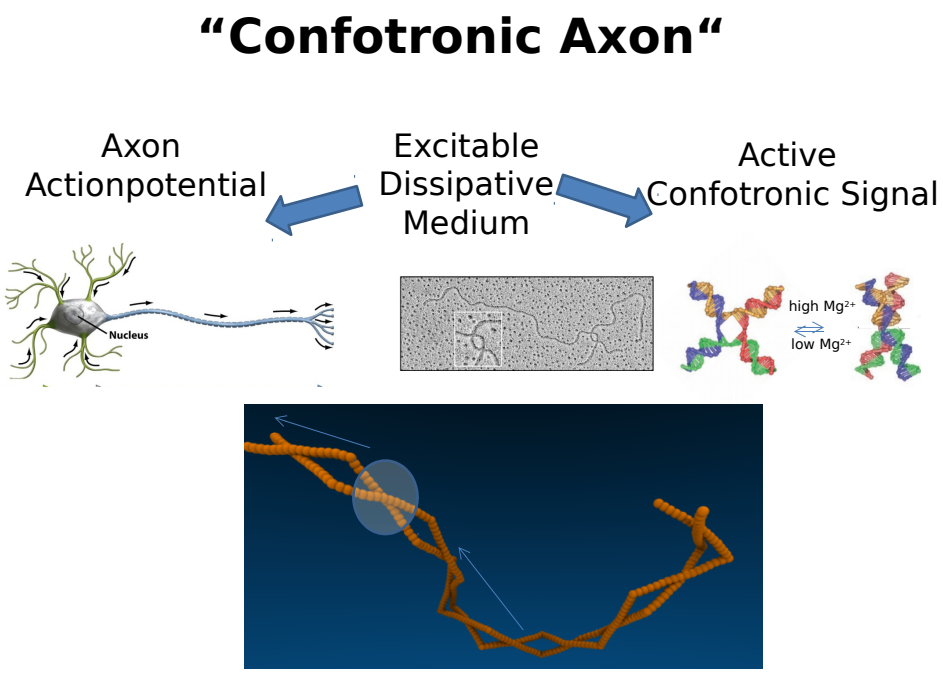

Figure 4.2: The axon and its envisioned confotronic counterpart: A synthetic confotronic fiber based on DNA Holliday junction geometry.

by the emerging field of DNA nanotechnology.

Finally, a number of HYPER drives could act cooperatively in small groups (10s of motor units) . We estimate an approximate addition of torques under certain parameter conditions. In particular in a certain range of electric field driving frequencies, ionic strength, pH, temperature, sizes of beads and motor grafting densities the HYPER drives will beneficially cooperate and significantly increase torques between the surfaces beyond that of a single unit.

4.2.2 DNA Nanomachines II: Synthetic Confotronic Fibers

Many biofilaments in Nature act as molecular information processing machines through cooperative (allosteric) coupling in their conformational dynamics. The central biophysical question in such systems is how do the protein monomer units establish their conformational interactions and coordinate their response to external stimuli. In a currently running project with colleagues at IPCMS and a PhD student we are attempting to recreate allostery in a synthetic system from scratch. We are assembling DNA based nanostructures forming dimers (soon oligomers and polymers) with the intrinsic ability to signal and ”copy” confor-

mational information between neighboring units. We are beginning to investigate the allosteric switching behavior of single DNA nanofibers using gel electrophoresis and magnetic tweezers force spectroscopy. Our ultimate long term vision is to create first "confotronic fibers" i.e. artificial mechano-nanowires able of transmitting molecular information over long distances beyond one micron.

The approach that we follow is to utilize ideas from DNA nanotechnology which is a rapidly growing field of interdisciplinary science. We in particular use the concepts of nano-origami[34] for assembling virtually arbitrary branched DNA structures out of simple single strand oligomers.

Our basic switchable monomer unit is a 4 arm Holliday junction that can undergo a switch between a stacked and an open state. Connecting such a unit to second identical one leads to a conformational coupling dictated by the geometry and mutual connection of the two units. We expect to see a very strong cooperativity of our DNA dimers and oligomer constructs in near future. Observing a cooperative domino-like cascade switching of a whole long fiber (by MT) will be an exciting event that we expect to observe in the course of the experiment. Once this goal is reached we plan to couple the monomer switching step to a non-equilibrium reaction, that will lead to an active autonomous propagation of the switching signal. Thus we will attempt to build a DNA analogue of an active neuronal fiber (axon) on the molecular scale.

As once said "There is nothing more practical than a theory". One could add to that: There is nothing more human(e) than technology[1].

[1]Of course the converse is true as well (making technology the most morally-bi-modal feature/bug of mankind).

Appendix A

APPENDICES

A.1 Toy-Model of Confotronics

Here we consider a simple but paradigmatic example for conceptual confotronics: Monomers are characterized by an internal **switching variable** "σ" that is governed by a **bistable** potential $U(\sigma)$. These non-linear switching variables are coupled to each other via linear **elastic degrees of freedom**, call them "h", in the medium they are embedded in. If we now consider the switches σ as frozen-in and formally calculate their elastic response function within the surrounding medium we can effectively integrate out the linear elastic medium from the system. That is, we can eliminate most degrees of freedom and we are left with only the switching variables σ and their longer range , elasticity induced **effective interactions**. At this level of coarse-graining we can then introduce dissipative dynamics and consider how switching-fronts and pulses propagate along these 1D systems.

The resulting dynamics is similar to autowaves in dissipative soliton systems. Such solitons have a definite velocity, set by the switching energy on the one hand and dissipation (fluid friction) on the other. Interestingly there is an analogy with the action potential propagation along neuronal axons. If conformational transitions of this sort can be realized within a switchable polymer one could rebuild an axon axon analogue based on a different information carrying mechanism with similar speeds of information transmission, yet nanoscopically small.

A.1.1 Switchable unit

Let's play through the program above on a very simple 1D filament of switchable units: Consider a monomer with internal conformational states described by a binary switching variable σ . The latter is a continuous variable but energetically prefers two values $\sigma \approx \pm 1$ where $+1$ reprents the "on" state and -1 the "off" state of the monomer. The two monomer states can in general have in different free energies in a bistable free energy landscape $U(\sigma)$. The shape of this potential

suppresses intermediate states between σ_1 and σ_2. For the sake of concreteness we can think of U of a quartic polynomial with a form like

$$\frac{U}{U_0} = \frac{x^4}{4} - \frac{1+a}{3}x^3 + \frac{a}{2}x^2 \quad (A.1)$$

$$x = \frac{\sigma+1}{2} \quad (A.2)$$

Here for convenience we redefined the Ising type variable σ into (binary type) x - moving now in the range between 0 and 1 (rather than -1 and +1). The shape of U is controlled by the parameter[1] a.

A.1.2 Elimination of Elastic Variables and Effective Interaction

Now lets consider the interaction of two such switches,σ_1 and σ_2 that are embedded in an elastic medium and spatially separated by some vector $\Delta\vec{r} = \vec{r}_1 - \vec{r}_2$. The quantity that captures their interaction is the coupling energy $E(\sigma_1, \sigma_2, \Delta\vec{r}) = -J(\Delta\vec{r})\,\sigma_1\sigma_2$. The distance- and medium-dependent coupling parameter J , gives rise to positive cooperativity when $J > 0$ and negative one for $J < 0$.

How does such a coupling $J(\Delta\vec{r})$ look like in concrete cases?

In a minimalistic model system we can consider a filament consisting of units which can switch their height in lateral direction to the filament axis -parametrized by the arc-length s (cf the Fig. 3.2, at the beginning of the manuscript). The units have preferred height depending on their switching variable σ:

$$h_\sigma(s) = \frac{h_+ + h_-}{2} + \frac{h_+ - h_-}{2}\sigma(s) \quad (A.3)$$

That says that the internal (confotronic) variable σ gives rise to an external (elastic) variable h

Let us for simplicity consider a material with a Poisson ration $\nu = 0$, for which the switch of height does not lead to a longitudinal length change in the perpendicular direction(s). If now a particular monomer switches its state and thus height to $h(s)$ and its neighbor has a different height $h(s+b)$ then in addition to the height change $h - h_\sigma$ from preferred one, there is also an additional shear deformation τ of the order $\frac{h(s+b)-h(s)}{b} \approx \frac{dh}{ds}$. This leads to an **elastic deformational energy** of the form

$$E_{el.def.} = \frac{1}{2}\int Y(h - h_\sigma)^2 + \mu b^2 \left(\frac{dh}{ds}\right)^2 ds$$

[1] In the $a \in (0,1)$ range $U(x)$ has two local minima, at $x = 0$ and 1 ($\sigma = \pm 1$) respectively and a barrier in-between them at $x = a$, with the barrier energy (w.r.t. the $x = 0$ state) of $U_{x=a} - U_{x=0} = \frac{U_0}{6}a^3(1-a)$. The energetic difference between the two states is $\Delta U = U_{x=1} - U_{x=0} = \frac{U_0}{6}\left(a - \frac{1}{2}\right)$. For $a = \frac{1}{2}$ the two states have equal energies and the potential becomes symmetric around the x=1/2 axis.

Here Y is the Young modulus, $\mu = Y/2$ the shear modulus and b the lattice constant (distance of neighbors along s). For an imposed monomer state (and thus $h_\sigma(s)$) we can write down the Euler-Lagrange equation (from the first variation of the elastic energy)

$$\lambda^2 h'' - h = -h_\sigma$$

with the characteristic decay length of deformation$\lambda = b\sqrt{\mu/Y}$. For the most general preferred deformation $h_\sigma(s)$ the solution can be written down as

$$h(s) = \int_{-\infty}^{+\infty} h_\sigma(\xi)\, G(s-\xi)\, d\xi \tag{A.4}$$

with the **spatial deformation propagator** (or elastic Green's function) given by

$$G(s-\xi) = \frac{1}{2\lambda} \exp\left(-\frac{|s-\xi|}{\lambda}\right) \tag{A.5}$$

Using the relations

$$\begin{aligned} \int G(s-\xi)\, G(s-\xi')\, ds &= \frac{(|\xi'-\xi|/\lambda + 1)}{4\lambda} e^{-|\xi'-\xi|/\lambda} \\ \int G'(s-\xi)\, G'(s-\xi')\, ds &= \frac{(-|\xi'-\xi|/\lambda + 1)}{4\lambda} e^{-|\xi'-\xi|/\lambda} \end{aligned}$$

and reinserting them into the interaction energy we obtain the elastic energy in its practical form

$$E = -\frac{Y}{4\lambda} \int\int h_\sigma(\xi)\, e^{-|\xi-\xi'|/\lambda} h_\sigma(\xi')\, d\xi d\xi' + \frac{Y}{2} \int h_\sigma^2(\xi)\, d\xi$$

This expression decomposes into two terms. The second, self-energy term is the energy penalty of switching of any point-switch ($h_\sigma(\xi)$) coming from the infinite elastic medium distortions. The rest is the pure interaction energy term

$$\begin{aligned} E_{int} &= -\int\int j(\xi-\xi')\, \sigma_1(\xi)\, \sigma_2(\xi')\, d\xi d\xi' \quad \text{with} \\ j(\xi-\xi') &= \frac{(h_+ - h_-)^2 Y}{16\lambda} e^{-|\xi-\xi'|/\lambda} \end{aligned}$$

Note that we have completely eliminated the elastic variable h from the picture. The only quantities remaining are the switches σ and their spatial interaction operator j. The switches are dressed in elastic variables which however become invisible in this representation.

For two short blocks of length $b \ll \lambda$ (or simply monomers) at a distance x from each other the two-monomer-interaction energy from above can be approximated as:

$$J_b(x) \approx \frac{(h_+ - h_-)^2 b^2 Y}{16\lambda} e^{-\frac{x}{\lambda}} \tag{A.6}$$

We see that for this elementary model the interaction energy is positive, in the Ising jargon "ferromagnetic". Note also that (at least in this simple 1D case) , J is quickly decaying on the characteristic elastic screening length λ.

To simplify the picture even further, it is practical to perform a little bit of further coarse-graining. The simplification consist of assuming a continuum approach, considering gradients like "$\frac{d\sigma}{ds}$" instead of discrete lattice values. Furthermore, zooming-out to length scales beyond the elastic coupling length λ, the height field h can be considered as slaved to σ, i.e. determined by the local value $\sigma(s)$ at the same position[2]. In such a coarse-grained limit, reintroducing the switching potential U we can write the energy of the system as

$$E = \int U(\sigma)\, ds + E_{int} \tag{A.7}$$

The interaction energy can be approximated by a squared gradient measuring the spacial variation of σ

$$E_{int} = \frac{K}{2} \int \left(\frac{d\sigma}{ds}\right)^2 ds$$

with K effective the confotronic stiffness. Noting that in our course-grained picture , the characteristic (mechanical screening) length λ replaces the monomer scale b and becomes the only relevant length scale here, the stiffness K can be approximated by assuming two neighboring coarse grained blocks of size $b \approx \lambda$ in Eq. A.6

$$K \approx \frac{(h_+ - h_-)^2 \lambda^2}{16} Y \tag{A.8}$$

A.1.3 Dynamics: Reaction -Diffusion Paradigm

To finally formulate the dynamic equations of motion, besides the energy A.7, we need to specify a concrete source of dissipation. We can assume the simplest form of power dissipation resulting from the local motion of the elastic variable $h \approx h_\sigma(s)$ (which here is locked-in toσ) through the fluid of vicosity η. The Rayleigh dissipation functional can be here written as $R_{diss} = \frac{\eta}{2} \int \left(\frac{dh}{dt}\right)^2 ds$ and in terms of σ

$$R_{diss} = \frac{\eta (h_+ - h_-)^2}{8} \int \left(\frac{d\sigma}{dt}\right)^2 ds$$

With $\dot{\sigma} = d\sigma/dt$, the equation of motion is then given by $\frac{\delta R_{diss}}{\delta \dot{\sigma}} = -\frac{\delta E}{\delta \sigma}$ or

$$\frac{\eta (h_+ - h_-)^2}{4} \dot{\sigma} = K \frac{d^2\sigma}{ds^2} - \frac{\partial U}{\partial \sigma} \tag{A.9}$$

[2]Mathematically , this is a consequence of the Greens-function becoming a delta function $G(x) \approx \delta(x)$ for $\lambda \to 0$.

Rescaling both sides of Eq. A.9 and switching to the (0-1-range) variable $x = \frac{\sigma+1}{2}$ we obtain

$$\dot{x} = D\frac{d^2x}{ds^2} + f(x) \tag{A.10}$$

and we recognize a reaction diffusion equation , with the (elasto-hydrodynamic) "diffusion constant"

$$D = \frac{\lambda^2 Y}{4\eta}$$

and a "reaction term" given from differentiating Eq. A.1

$$f(x) = f_0 x(a-x)(x-1) \tag{A.11}$$

with

$$f_0 = \frac{1}{t_0} = \frac{U_0}{\eta(h_+ - h_-)^2}$$

a characteristic relaxation frequency defining the relaxation time t_0.

Note here, that unlike the standard stochastic mass-diffusion, our diffusion process here is a fully deterministic, elasto-hydrodynamic deformation spread. The "reaction term" lookalike f stems from a mechanical restoring force acting on the switching variable x (i.e. σ). Yet, apart from this difference in interpretation, the equation A.10 shares much common physics with a classical reaction diffusion equation. This analogy seems very attractive as it opens up the possibility of seeing the confotronic fiber as an "excitable medium" able of transmitting autowaves down its contour. The autowaves, which are also sometimes referred to as "dissipative solitons", are out-of.equilibrium, non-linear moving excitations in a reaction diffusion equation or more generally in a system of several coupled equationsA.10.

A.1.4 Confotronic Autowaves, Traveling Fronts

Looking at Eq. A.10 we see that the product of the elasto-diffusion constant D and the relaxation time t_0 sets on the other hand a characteristic length-scale

$$l_0 = \sqrt{Dt_0} = \lambda\sqrt{\frac{Y(h_+ - h_-)^2}{4U_0}}$$

that together with t_0 gives rise to a characteristic velocity scale

$$v_0 = l_0/t_0 = \frac{\lambda\sqrt{YU_0}}{2\eta(h_+ - h_-)}.$$

Thus a stiffer elastic medium and deeper switching pontential ,with Y and U_0 larger (i.e. for stronger driving forces) as well as lower viscosity η or smaller displacements $h_\pm$ (lowever dissipation) naturally give rise to larger velocities. For a typical system with monomer size b of few nm and λ in the range of $10nm$ we can estimate $U_0 \sim 10kT/10nm = 4pN$, $Y \sim 100MPa$ (modulus of typical

proteins), $(h_+ - h_-) \sim 1nm$, $\eta = 10^{-3} Pa \cdot s$ (typical aqueous solvent) we get $U_0 \sim 4pN$, $l_0 \sim 25nm$, $t_0 \sim 2.5 \times 10^{-10} s$ and $v_0 \sim 100 \frac{m}{s}$. This velocity is very high , but what is its actual meaning ?

To answer that, we note that the equation of the form A.10 with A.11 appears in the context of a simplified model of nerve impulse propagation along axons and is also known as the Nagumo equation [151]. It posses traveling front solutions of the form:

$$x(s,t) = \left(1 + \exp\left(-\frac{s + ct}{\sqrt{2} l_0}\right)\right)^{-1} \tag{A.12}$$

as can be checked by direct insertion. For $0 < a < 1/2$,where the $x = 1$ ($\sigma = -1$) state is more favorable, a switch propagates from $x = 0$ to $x = 1$ state with the speed

$$c = \sqrt{2}\left(\frac{1}{2} - a\right) v_0$$

For $a > 1/2$ the $x = 0$ state becomes more favorable and the propagation direction inverts ($c < 0$). For $a = 1/2$ the two states have equal energies and naturally in the absence of any driving force the front does not propagate i.e. $c = 0$.Taking the characteristic velocity v_0 estimate from above and a typical case of $a = \frac{1}{4}$ we get $c \sim 35 \frac{m}{s}$. This notable speed[3] is comparable to velocities of nerve impulses traveling along axons.

A.1.5 Traveling Pulses

In our confotronic system simple a traveling front (TF) can be transmitted if the system is prepared in a metastable state. But once the system has switched to the energetically lower state it would need to be reset to the initial state to operate once again. This would put serious limitations to the actual usefulness of such a fiber in applications of information transmission at the nanoscale. Can one do better that generating a one way TF? An other type of autowaves are traveling pulses (TPs), like those running along our neuronal axons. TPs are intrinsically "resetting" themselves by running through a transient excitation - deexcitation cycle. Could one regenerate such a TPs in a confotronic system? It turns out that a simple one variable diffusion-reaction equation is not able to transmit TPs [150]. It does not have enough dynamic complexity. However a slight modification of the Nagumo system which involves a second spacio-dynamic variable turns out to be complex enough to generate TP.

Imagine a system described by Eq. A.10 which is now coupled to a chemical energy reservoir, like ATP[4] If we assume that ATP can bind to one conformation

[3] It is so high that we might even leave the low Reynolds number regime (Re$\sim$ 1 for the given l_0, v_0 and η). This indicates that the for traveling front propagation along a confotronic filament the (here neglected) inertial effects of the solvent along the chain might become relevant.

[4] ATP is an ubiquitous energy source throughout living nature. ATP is split spontaneously

and induce the preference to switch to the other state, the coupled equations for the fraction of binding sites occupied with ATP by A

$$\begin{aligned} \dot{x} &= D\frac{d^2x}{ds^2} + f(x) - A \\ \dot{A} &= c_1 x - c_2 A \end{aligned}$$

The constants c_1 and c_2 are related to the binding rate of ATP to the $x = 1$ state and the spontaneous decay of ATP binding respectively[5].

This extension of the Nagumo equation is also known as the Nagumo-FitzHugh model and is **the** generic toy model for axonal spikes.

A.2 Animas as Motors

From the previous examples (in the chapter on animotion) we have learned that there are two distinct classes of animas: those who run easily and unidirectionally (type 1) and those, bi-directional ones that need to break a symmetry to decide which way they run (type 2 animas). The distinction is not a mere mathematical subtlety. It touches upon the practical utility of the anima as motors. A device that inverts its direction upon weak opposition in its surrounding is dynamically less robust than an object that turns unidirectionally and without any threshold[6].

The general motility behavior of animas is essentially characterized by their dissipative "kinematic" relation. By this we mean the relation between the energy "pumping" rate (represented by p), the energy "dumping" rates in form of friction or heat dissipation (cf. $\tau_e$and r) and the induced velocity (ω). Examples of such kinematic relations are Eqs.3.183.24 and 3.29. Going beyond the pure kinematics, animas true single piece motors that can be characterized by a *dynamic relation or "motor equation"*. The dynamic relation describes the connection between all energy in- and out-fluxes with the generalized force it can apply to its surroundings. For animas whose animodes are associated with angular variables this generalized force is in fact a torque. The dynamic relation

into ADP and a phosphate group P, reducing its free energy (at sufficiently low concentration of ATP).

[5]Note that in general these two constants need not obey any thermodynamic relation, as the possibility of ATP chemical breakup (hydrolysis) pushes the system away from the equilibrium.

[6]The "without threshold" statement for type 1 animas has however to be taken with a grain of salt and is true only in absence of an external torque and in absence of dry friction. So far we have ignored dry friction which can naturally induce a threshold even in a system that does not break symmetry. Although dry friction has something of an analytical nuisance -due to its singular velocity independent nature- it is basically always present. It is often even dominant over other forms of friction on the macroscopic scale and small speeds. Not surprisingly dry friction modifies the onset of animotion, such that there is always a minimal pumping threshold that needs to overcome the constant friction force. Leaving technical details to later work one can still state, that apart from the shift of onset, animotion keeps its character regardless of particular type of friction.

can be obtained by simply adding an additional (external) torque term to the torque balance, i.e. to the right hand side of Eqn. 3.10. For the three anima types from above the dynamic relations for the scaled torque $m = \frac{LM}{4\pi^2 B}$ can be expressed as:

$$m = \omega - \frac{pr}{\tau_e(\omega^2 + r^2)} \tag{A.13}$$

for the type 1 anima ring drive from below. For the ring driven from inside (type 2 anima) we have

$$m = \omega - \frac{p\omega}{\tau_e(\omega^2 + r^2)} \tag{A.14}$$

Finally for the fiber/spaghetti (type 2) anima we obtain similarly:

$$m = \omega - \frac{p^2 r\omega}{\tau_e(\omega^2 + r^2)^2} \tag{A.15}$$

These dynamic relations contain the corresponding kinetic relations as special cases for vanishing external torque $m = 0$. For large toques of any sign $|m| \gg 1$ the angular velocity in all three cases follows the external torque $m \simeq \omega$. That is, large torques can overcome any internal drive and dictate the motion. This finding is unsurprising, as the animas respond only passively in this regime. The real beauty lies in the subtle differences of the second terms on the r.h.s., that show up for smaller torques for which the internal drive competes with the external torque.

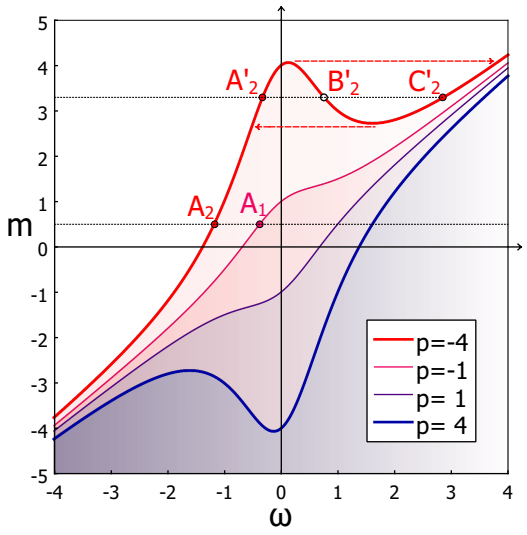

Figure A.1: The dynamic relation of typical type 1 animas (e.g. torus on a hot surface).

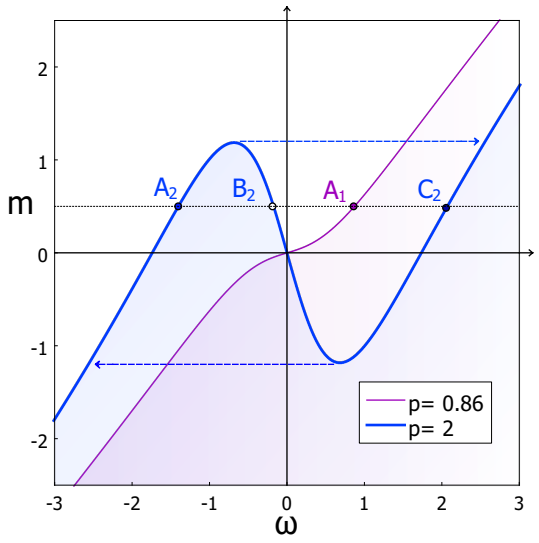

Figure A.2: The dynamic relation of a typical type 2 anima - the spaghetti motor.

Bibliography

[1] R. Dawkins, Why don't animals have wheels? Sunday Times, November 24, (1996)

[2] I.M.Kulić, R. Thaokar and H. Schiessel, Twirling DNA rings - Swimming nanomotors ready for a kickstart, Europhys. Lett. 72, 527 (2005)

[3] Balzani, Venturi & Credi, Molecular Devices and Machines, Wiley-VCH (2003)

[4] J. M. Berg, J. L. Tymoczko and L. Stryer . Biochemistry. 5th edition. W. H. Freeman

[5] Direct observation of the rotation of F1-ATPase, H. Noji, R. Yasuda, M. Yoshida, and K. Kinosita, Nature, 386, 299-302 (1997).

[6] H.C. Berg & R.A. Anderson, Bacteria Swim by Rotating their Flagellar Filaments, Nature 245, 380 (1973);

[7] A. Maxwell and A. D. Bates, DNA topology, Oxford University Press, 2005

[8] C. Mao, W. Sun, Z. Shen and N. C. Seeman,A nanomechanical device based on the B–Z transition of DNA, Nature, 397, 144-146 (1999)

[9] H. Yan, X. Zhang, Z. Shen and N. C. Seeman, A Robust DNA Mechanical Device Controlled by Hybridization Topology, Nature 415, 62–65 (2002)

[10] N. Koumura, R. W. J. Zijlstra, R. A. van Delden, N. Harada and B. L. Feringa, Light-driven monodirectional molecular rotor, Nature 401, 152-155 (1999)

[11] T. R. Kelly, H. De Silva and R. A. Silva, Unidirectional rotary motion in a molecular system, Nature 401, 150 1999.

[12] J-M. Lehn, Conjecture: Imines as Unidirectional Photodriven Molecular Motors—Motional and Constitutional Dynamic Devices, Chem. Eur. J., 12: 5910–5915 (2006)

[13] P. G. de Gennes, Scaling concepts in polymer physics. Cornell University Press, Ithaca (1979)

[14] De Gennes, P. G. Entangled polymers. Physics Today 36 (6): 33–31. (1983).

[15] M. Doi & S. Edwards, The Theory of Polymer Dynamics, Clarendon Press (1999)

[16] F. Spitzer, Some Theorems Concerning 2-Dimensional Brownian Motion, Trans. Am. Math. Soc. 87, 187-97 (1958)

[17] S. Prager and H.L. Frisch, Statistical Mechanics of a Simple Entanglement, J. Chem. Phys. 46, 1475 (1967)

[18] S.F. Edwards, Statistical mechanics with topological constraints: I, Proc. Phys. Soc. London 91, 513 (1967)

[19] J. Rudnick and Y.Hu, The winding angle distribution of an ordinary random walk, J. Phys. A: Math. Gen. 20 4421-4438 (1987).

[20] A. Grosberg and H. Frisch, Winding angle distribution for planar random walk, polymer ring entangled with an obstacle, and all that: Spitzer–Edwards–Prager–Frisch model revisited, J. Phys. A 36, 8955 (2003)

[21] C. Walter, G.T. Barkema, and E. Carlon, The equilibrium winding angle of a polymer around a bar, J. Stat. Mech. P10020 (2011)

[22] J.F. Marko, Linking topology of tethered polymer rings with applications to chromosome segregation and estimation of the knotting length, Phys. Rev. E 79, 051905 (2009)

[23] T. R. Strick, J.-F. Allemand, D. Bensimon, A. Bensimon and V. Croquette, The Elasticity of a Single Supercoiled DNA Molecule, Science 29, 1835 (1996)

[24] J. F. Marko and E. D. Siggia, Fluctuations and supercoiling of DNA, Science 265, 506 (1994); Statistical mechanics of supercoiled DNA,Phys. Rev. E 52, 2912 (1995)

[25] J.-C. Walter, M. Baiesi, E.Carlon and H. Schiessel, Unwinding Dynamics of a Helically Wrapped Polymer, Macromolecules 47, 4840 (2014)

[26] J.F. Marko, Supercoiled and braided DNA under tension, Phys. Rev. E 55, 1758 (1997)

[27] Ball, R. C., Doi, M., Edwards, S. F. & Warner, M. Elasticity of entangled networks, Polymer 22,1010–1018 (1981); P. G. de Gennes, Sliding gels, Physica A 271,231–237 (1999);

[28] Harada, A. & M.Kamachi,Complex formation between poly(ethylene glycol) and a-cyclodextrin, Macromolecules 23, 2821–2823 (1990); Okumura,Y. & Ito, K., The polyrotaxane gel: a topological gel by figure-of-eight cross-links, Adv. Mater 13,485–487 (2001)

[29] T.C. Boles, J.H. White, and N.R. Cozzarelli, Structure of plectonemically supercoiled DNA, J. Mol. Biol.213(1990), no. 4, 931–51

[30] N.R. Cozzarelli, T. Christian-Boles, and James H. White, Primer on the topology and geometry of DNA supercoiling, DNA Topology and its Biological Effects (1990), 139–184

[31] T. Sanchez, I. M. Kulić, and Z. Dogic, Circularization, Photomechanical Switching, and a Supercoiling Transition of Actin Filaments, Phys. Rev. Lett. **104**, 098103 (2010).

[32] I. M. Kulić, Evaluating polynomials on the molecular level - a novel approach to molecular computers, Biosystems 45, 45 (1998)

[33] M. Shahinpoor, K.J. Kim and M. Mojarrad, Artificial Muscles: Applications of Advanced Polymeric Nanocomposites. Taylor & Francis (New York, London) (2007)

[34] N.C. Seeman. "Nanotechnology and the double helix". Scientific American 290 (6): 64–75 (2004)

[35] Paul W. K. Rothemund,Folding DNA to create nanoscale shapes and patterns, Nature 440, 297-302 (2006)

[36] F. C. Simmel and Y. Krishnan, Nucleic Acid Based Molecular Devices, Angew. Chem. Int. Ed. 50, 3124 (2011)

[37] SM Douglas, H Dietz, T Liedl, B Hogberg, F Graf, and WM Shih, Self-assembly of DNA into nanoscale three-dimensional shapes. Nature 459, 414 (2009) ; Hendrik Dietz, S. M. Douglas, W. M. Shih, Folding DNA into Twisted and Curved Nanoscale Shapes, Science 325,725 (2009)

[38] B. Yurke, A.J. Turberfield, A.P. Mills, F.C. Simmel, J.L. Neumann, A DNA-fuelled molecular machine made of DNA. Nature. 406, 605 (2000); S.F. Wickham, J. Bath, Y. Katsuda, M. Endo, K. Hidaka, H. Sugiyama, A.J. Turberfield, A DNA-based molecular motor that can navigate a network of tracks, Nat Nanotechnol 7, 169 (2012)

[39] P. Pieranski, In search of ideal knots. In: Ideal Knots, Series on Knots and Everything, A. Stasiak, V. Katritch and L.H. Kauffman (eds), Vol. 19., pp. 20–41, World Scientific, Singapore (1998).

[40] S. Neukirch and G.H.M. Van der Heijden, Geometry and Mechanics of Uniformn-Plies: from Engineering Ropes to Biological Filaments, J. Elast. 69: 41–72 (2002)

[41] F. Weisser, O. Benzerara, A. Johner and I.M. Kulić, Topological energy storage of work generated by nanomotors , Soft Matter 11, 732 (2015)

[42] Q. Li, G. Fuks, E. Moulin, M. Maaloum, M. Rawiso, I.M. Kulić, J.T. Foy and N. Giuseppone, Macroscopic Contraction of a Gel Induced by the Integrated Motion of Light-Driven Molecular Motors, Nature Nanotech. 10, 161 (2015)

[43] Z. Chen et al. Nonlinear Geometric Effects in Mechanical Bistable Morphing Structures , PRL 109,114302 (2012); Q. Guo, A. K. Mehta, M. A. Grover, W. Chen, D. G. Lynn, and Z. Chen, Shape Selection and Multistability in Helical Ribbons, Applied Physics Letters 104, 211901 (2014);

[44] S. Armon, H. Aharoni, M. Moshe, and E. Sharon, Shape selection in chiral ribbons: from seed pods to supramolecular assemblies. Soft Matter ,10,2733 (2014)

[45] Y. Forterre, J. M. Skotheim, J. Dumais, and L. Mahadevan,How the Venus flytrap snaps , Nature 433, 421–425 (2005)

[46] Mohrbach, H., A. Johner, and I. M. Kulic. 2010. Tubulin bistability and polymorphic dynamics of microtubules. *Phys. Rev. Lett.* 105:268102.

[47] H. Mohrbach , A.Johner and I.M. Kulić. Cooperative lattice dynamics and anomalous fluctuations of microtubules. Eur. Biophys. J. Biophys. Lett., 41, 217 (2012)

[48] Ziebert, F., Mohrbach, H., & Kulic, I. M. Why Microtubules Run in Circles: Mechanical Hysteresis of the Tubulin Lattice. Phys. Rev. Lett., 114, (2015)

[49] Howard, J., Mechanics of Motor Proteins and the Cytoskeleton, Sinauer Press 2001.

[50] Amos, L. A., and Amos W. G., Molecules of the Cytoskeleton, Guilford Press 1991.

[51] Kulic, I. M., A. E. X. Brown, H. Kim, C. Kural, B. Blehm, P. R. Selvin. 2008. The role of microtubule movement in bidirectional organelle transport. *Proc. Natl. Acad. Sci. USA*. 105:10011-10016.

[52] Alberts, B., A. Johnson, J. Lewis, M. Raff, K. Roberts, and P. Walter. 2005. Molecular Biology of the Cell.

[53] Nogales, E., M. Whittaker, R. A. Milligan, K. H. Downing 1999. High resolution model of the microtubule. *Cell*. 96:79-88.

[54] Huilin, J., D. J. DeRosier, W. V. Nicholson, E. Nogales, K. H. Downing. 2002. Microtubule Structure at 8 $\mathring{A}$ Resolution. *Structure*. 10:1317-1328.

[55] Nogales, E., S. G. Wolf, and K. H. Downing. 1998. Structure of the $\alpha\beta$ tubulin dimer by electron crystallography. *Nature.* 391:199-203.

[56] Löwel, J., H. Li, K. H. Downing and E. Nogales. 2001.Refined Structure of $\alpha\beta$-Tubulin at 3.5 $\mathring{A}$ Resolution. *J. Mol. Biol.* 313:10451-057.

[57] Bouchet-Marquis, C., B. Zuber, A-M. Glynn, M. Eltsov, M. Grabenbauer, K. N. Goldie, D. Thomas, A. S. Frangakis, J. Dubochet, and D. Chrétien. 2007. Visualization of cell microtubules in their native state. *Bio. Cell.* 99:45-53.

[58] Wade, R. H., D. Chrétien, and D. Job. 1990. Characterization of microtubule protofilament numbers. How does the surface lattice accommodate?. *J. Mol. Bio.* 212:775-786.

[59] Chretien, D., and R. H. Wade. 1991. New data on the microtubule surface lattice. *Bio. Cell. 71*:161-174.

[60] Ray, S., E. Meyhofer, R. A. Milligan, and J. Howard. 1993. Kinesin follows the microtubule's protofilament axis. *J. Cell Biol.* 121:1083-1093.

[61] Chrétien, D., F Metoz, F Verde, E Karsenti, and R. H. Wade. 1992. Lattice defects in microtubules: protofilament numbers vary within individual microtubules. *J. Cell. Biol.* 117:1031-1040.

[62] Chretien, D., and S. D. Fuller. 2000. Microtubules switch occasionally into unfavorable configurations during elongation. *J. Mol. Biol.* 298:663-676.

[63] Hunyadi, V., I. M. Janosi. 2007. Metastability of Microtubules Induced by Competing Internal Forces. *Biophys. J.* 92:3092-3097

[64] Mandelkow, E. M., E. Mandelkow, R. A. Milligan. 1991. Microtubules dynamics and microtubules caps: a time-resolved cryoelectron microscopy study. *J. Cell. Biol.* 114:977-991.

[65] Nogales, E., H. W. Wang, H. Niederstrasser. 2003. Tubulin rings: which way do they curve ?. *Curr. Opin. Struct. Biol.* 13:256-261.

[66] Mitchison, T., and M. W. Kirschner. 1984. Dynamic instability of microtubule growth. *Nature.* 312:237-242.

[67] Erickson, H. P., and E. T. O'Brien. 1992. Microtubule dynamic instability and GTP hydrolysis. *Annu. Rev. Biophys. Biomol. Struct.* 21:145-166.

[68] Janosi, I. M., Chretien, D. and Flyvbjerg, H. 2002. Structural microtubule cap: stability, catastrophe, rescue, and third state. *Biophys. J.* 83:1317-1330.

[69] Arnal, I., and R. H. Wade. 1995. How does taxol stabilize microtubules ?. *Curr. Biol.* 5:900-908.

[70] Amos, L. A., and J. Löwe. 1999. How taxol stabilises microtubule structure. *Chem. Biol.* 6:R65-R69.

[71] Xiao, H., P. Verdier-Pinard, N. Fernandez-Fuentes, B. Burd, R. Angeletti, A. Fiser, S. B. Horwitz, G. A. Orr. 2006. Insights into the mechanism of microtubule stabilization by taxol. *Proc. Natl. Acad. Sci. USA*. 103:10166-10173.

[72] Elie-Caille, C., F. Severin, J. Helenius, J. Howard, D. J. Muller, A. A. Hyman. 2007. Straight GDP-tubulin protofilaments form in the presence of taxol. *Curr. Biol.* 17:1765-1770.

[73] Gittes, F., B. Mickey, J. Nettleton, and J. Howard. 1993. Flexural rigidity of microtubules and actin filaments measured from thermal fluctuations in shape. *J. Cell Biol.* 120:923-934.

[74] Venier, P., A. C. Maggs, M. F. Carlier, and D. Pantaloni. 1994. Analysis of microtubule rigidity using hydrodynamic flow and thermal

fluctuations. *J. Biol. Chem.* 269:13353

[75] Mickey, B., and J. Howard. 1995. Rigidity of microtubules is increased by stabilizing agents. *J. Cell Biol.* 130:909-917.

[76] Felgner, H., R. Frank, and M. Schliwa. 1996. Flexural rigidity of microtubules measured with the use of optical tweezers. *J. Cell Sci.* 109:509-516.

[77] Kikumoto, M., M. Kurachi, V. Tosa, and H. Tashiro. 2006. Flexural rigidity of individual microtubules measured by a buckling force with optical traps. *Biophys. J.* 90:1687-1696.

[78] Kurachi, M., M. Hoshi, and H. Tashiro. 1995. Buckling of a single microtubule by optical trapping forces: direct measurement of microtubule rigidity. *Cell Motil. Cytoskeleton.* 30:221-228.

[79] Takasone, T., S. Juodkazis, Y. Kawagishi, A. Yamaguchi, S. Matsuo, H. Sakakibara, H. Nakayama, and H. Misawa. 2002. Flexural rigidity of a single microtubule. *Jpn. J. Appl. Phys.* 41:3015-3019.

[80] Kis, A., S. Kasas, B. Babic, A. J. Kulik, W. Benoit, G. A. Briggs, C. Schonenberger, S. Catsicas, and L. Forro. 2002. Nanomechanics of microtubules. *Phys. Rev. Lett.* 89:248101.

[81] Van den Heuvel, M. G. L., S. Bolhuis, and C.Dekker. 2007. Persistence length measurements from stochastic single-microtubule trajectories, *Nano Lett.* 7:3138.

[82] Van den Heuvel, M. G. L., M. P. de Graaff, and C. Dekker. 2008. Microtubule curvatures under perpendicular electric forces reveal a low persistence length. *Proc. Natl. Acad. Sci. USA* 105:7941.

[83] Kim, T., M. T. Kao, E. F. Hasselbrink, and E. Meyhöfer. 2008. Nanomechanical model of microtubule translocation in the presence of electric fields. *Biophys J.* 94:3880-3892.

[84] Pampaloni, F., G. Lattanzi, A. Jonas, T. Surrey, E. Frey, and E. L. Florin. 2006. Thermal fluctuations of grafted microtubules provide evidence of a length-dependent persistence length. *Proc. Natl. Acad. USA*. 103:10248-10253.

[85] Taute, K. M., F. Pampaloni, E. Frey, and E-L. Florin, 2008. Microtubule dynamics depart from the wormlike chain model. *Phys. Rev. Lett.* 100, 028102.

[86] Brangwynne, C., G. Koenderink, E. Barry, Z. Dogic, F. MacKintosh, and D. Weitz. 2007. Bending dynamics of fluctuating biopolymers probed by automated high-resolution filament tracking. *Biophys. J.* 93:346-359.

[87] Janson, M. E. and M. Dogterom. 2004. A bending mode analysis for growing microtubules: evidence for a velocity-dependent rigidity. *Biophys. J.* 87:2723-2736.

[88] Van den Heuvel, M. G. L., M. P. de Graaff, S. G. Lemay, and C. Dekker. 2007. Electrophoresis of individual microtubules in microchannels. *Proc Natl Acad Sci U S A*. 104:7770-7775.

[89] Amos, L. A., and W. B. Amos. 1991. The bending of sliding microtubules imaged by confocal light microscopy and negative stain electron microscopy. *J. Cell. Sci. Suppl.* 14:95-101.

[90] Vale, R.D., C. M. Coppin, F. Malik, F. J. Kull, and R. D. Milligan. 1994. Tubulin GTP hydrolysis influences the structure, mechanical properties and kinesin-driven transport of microtubules. *J. Biol. Chem.* 269:23769-23775

[91] Amos, L. A. Negative Stain electron microscopy of microtubules and associated motor molecules. 1991. *Micron and Microscopica Acta.* 22:395.

[92] R. Everaers, R. Bundschuh, and K. Kremer, Fluctuations and Stiffness of Double Stranded Polymers: Railway Track Model, Europhys.Lett. 29, 263 (1995)

[93] Heussinger, C., M. Bathe, and E. Frey. 2007. Statistical mechanics of semiflexible bundles of wormlike polymer chains. *Phys. Rev. lett.* 99:048101.

[94] Mohrbach, H., and I.M. Kulic. 2007. Motor driven microtubule shape fluctuations: force from within the lattice. *Phys. Rev. Lett.* 99:218102.

[95] G. M. Nam, N. K. Lee , H. Mohrbach, A. Johner and I.M. Kulić. Helices at interfaces. EPL 100, 28001 (2012).

[96] 7. J. Fierling, M. M. Müller, H. Mohrbach, A. Johner and I.M. Kulić, Crunching Biofilament Rings, EPL 107, 68002 (2014).

[97] 8. O . Kahraman, H. Mohrbach, M.M. Müller and I.M. Kulić, Confotronic dynamics of tubular filaments , SOFT MATTER, 10, 2836 (2014)

[98] Chrétien, D., H. Flyvbjerg, and S. D. Fuller. 1998. Limited flexibility of the inter-protofilament bonds in microtubules assembled from pure tubulin. *Eur Biophys* J 27:490-500.

[99] Asakura, S. 1970. Polymerization of flagellin and polymorphism of flagella. *Adv. Biophys. (Japan).* 1:99-155.

[100] Calladine, C. R. 1975. Construction of bacterial flagella. *Nature (London)* 255:121-124.

[101] Monod J., Wyman J., and Changeux J.-P. (1965). On the nature of allosteric transitions: a plausible model. J. Mol. Biol. 12: 88-118.

[102] Duke, T.A.J., N. Le Novere, and D. Bray (2001) 'Conformational spread in a ring of proteins: A stochastic approach to allostery'. Journal of Molecular Biology, 308(3): p. 541-553.

[103] D. S. Goodsell and A. J. Olson, Structural Symmetry and Protein Function , Ann. Rev. Bioph. Biomol. Struct. 29:105 (2000)

[104] E. Muto, H. Sakai and K. Kaseda. 2005. Long-range cooperative binding of kinesin to a microtubule in the presence of ATP. *J. Cell Biol.* 168:691.

[105] I.M.Kulić, R. Thaokar and H. Schiessel, Twirling DNA rings - Swimming nanomotors ready for a kickstart, Europhys. Lett. 72, 527 (2005)

[106] Balzani, Venturi & Credi, Molecular Devices and Machines, Wiley-VCH (2003)

[107] J. M. Berg, J. L. Tymoczko and L. Stryer . Biochemistry. 5th edition. W. H. Freeman

[108] Direct observation of the rotation of F1-ATPase, H. Noji, R. Yasuda, M. Yoshida, and K. Kinosita, Nature, 386, 299-302 (1997).

[109] H.C. Berg & R.A. Anderson, Bacteria Swim by Rotating their Flagellar Filaments, Nature 245, 380 (1973);

[110] A. Maxwell and A. D. Bates, DNA topology, Oxford University Press, 2005

[111] C. Mao, W. Sun, Z. Shen and N. C. Seeman,A nanomechanical device based on the B–Z transition of DNA, Nature, 397, 144-146 (1999)

[112] H. Yan, X. Zhang, Z. Shen and N. C. Seeman, A Robust DNA Mechanical Device Controlled by Hybridization Topology, Nature 415, 62–65 (2002)

[113] N. Koumura, R. W. J. Zijlstra, R. A. van Delden, N. Harada and B. L. Feringa, Light-driven monodirectional molecular rotor, Nature 401, 152-155 (1999)

[114] T. R. Kelly, H. De Silva and R. A. Silva, Unidirectional rotary motion in a molecular system, Nature 401, 150 1999.

[115] J-M. Lehn, Conjecture: Imines as Unidirectional Photodriven Molecular Motors—Motional and Constitutional Dynamic Devices, Chem. Eur. J., 12: 5910–5915 (2006)

[116] P. G. de Gennes, Scaling concepts in polymer physics. Cornell University Press, Ithaca (1979)

[117] De Gennes, P. G. Entangled polymers. Physics Today 36 (6): 33–31. (1983).

[118] M. Doi & S. Edwards, The Theory of Polymer Dynamics, Clarendon Press (1999)

[119] F. Spitzer, Some Theorems Concerning 2-Dimensional Brownian Motion, Trans. Am. Math. Soc. 87, 187-97 (1958)

[120] S. Prager and H.L. Frisch, Statistical Mechanics of a Simple Entanglement, J. Chem. Phys. 46, 1475 (1967)

[121] S.F. Edwards, Statistical mechanics with topological constraints: I, Proc. Phys. Soc. London 91, 513 (1967)

[122] J. Rudnick and Y.Hu, The winding angle distribution of an ordinary random walk, J. Phys. A: Math. Gen. 20 4421-4438 (1987).

[123] A. Grosberg and H. Frisch, Winding angle distribution for planar random walk, polymer ring entangled with an obstacle, and all that: Spitzer–Edwards–Prager–Frisch model revisited, J. Phys. A 36, 8955 (2003)

[124] C. Walter, G.T. Barkema, and E. Carlon, The equilibrium winding angle of a polymer around a bar, J. Stat. Mech. P10020 (2011)

[125] J.F. Marko, Linking topology of tethered polymer rings with applications to chromosome segregation and estimation of the knotting length, Phys. Rev. E 79, 051905 (2009)

[126] T. R. Strick, J.-F. Allemand, D. Bensimon, A. Bensimon and V. Croquette, The Elasticity of a Single Supercoiled DNA Molecule, Science 29, 1835 (1996)

[127] J. F. Marko and E. D. Siggia, Fluctuations and supercoiling of DNA, Science 265, 506 (1994); Statistical mechanics of supercoiled DNA,Phys. Rev. E 52, 2912 (1995)

[128] J.-C. Walter, M. Baiesi, E.Carlon and H. Schiessel, Unwinding Dynamics of a Helically Wrapped Polymer, Macromolecules 47, 4840 (2014)

[129] J.F. Marko, Supercoiled and braided DNA under tension, Phys. Rev. E 55, 1758 (1997)

[130] Ball, R. C., Doi, M., Edwards, S. F. & Warner, M. Elasticity of entangled networks, Polymer 22,1010–1018 (1981); P. G. de Gennes, Sliding gels, Physica A 271,231–237 (1999);

[131] Harada, A. & M.Kamachi,Complex formation between poly(ethylene glycol) and a-cyclodextrin, Macromolecules 23, 2821–2823 (1990); Okumura,Y. & Ito, K., The polyrotaxane gel: a topological gel by figure-of-eight cross-links, Adv. Mater 13,485–487 (2001)

[132] T.C. Boles, J.H. White, and N.R. Cozzarelli, Structure of plectonemically supercoiled DNA, J. Mol. Biol.213(1990), no. 4, 931–51

[133] N.R. Cozzarelli, T. Christian-Boles, and James H. White, Primer on the topology and geometry of DNA supercoiling, DNA Topology and its Biological Effects (1990), 139–184

[134] I. M. Kulić, Evaluating polynomials on the molecular level - a novel approach to molecular computers, Biosystems 45, 45 (1998)

[135] M. Shahinpoor, K.J. Kim and M. Mojarrad, Artificial Muscles: Applications of Advanced Polymeric Nanocomposites. Taylor & Francis (New York, London) (2007)

[136] N.C. Seeman. "Nanotechnology and the double helix". Scientific American 290 (6): 64–75 (2004)

[137] Paul W. K. Rothemund,Folding DNA to create nanoscale shapes and patterns, Nature 440, 297-302 (2006)

[138] F. C. Simmel and Y. Krishnan, Nucleic Acid Based Molecular Devices, Angew. Chem. Int. Ed. 50, 3124 (2011)

[139] SM Douglas, H Dietz, T Liedl, B Hogberg, F Graf, and WM Shih, Self-assembly of DNA into nanoscale three-dimensional shapes. Nature 459, 414 (2009) ; Hendrik Dietz, S. M. Douglas, W. M. Shih, Folding DNA into Twisted and Curved Nanoscale Shapes, Science 325,725 (2009)

[140] B. Yurke, A.J. Turberfield, A.P. Mills, F.C. Simmel, J.L. Neumann, A DNA-fuelled molecular machine made of DNA. Nature. 406, 605 (2000); S.F. Wickham, J. Bath, Y. Katsuda, M. Endo, K. Hidaka, H. Sugiyama, A.J. Turberfield, A DNA-based molecular motor that can navigate a network of tracks, Nat Nanotechnol 7, 169 (2012)

[141] P. Pieranski, In search of ideal knots. In: Ideal Knots, Series on Knots and Everything, A. Stasiak, V. Katritch and L.H. Kauffman (eds), Vol. 19., pp. 20–41, World Scientific, Singapore (1998).

[142] S. Neukirch and G.H.M. Van der Heijden, Geometry and Mechanics of Uniformn-Plies: from Engineering Ropes to Biological Filaments, J. Elast. 69: 41–72 (2002)

[143] en.wikipedia.org/wiki/Buttered_cat_paradox

[144] F. A. Samatey et al., Structure of the bacterial flagellar hook and implication for the molecular universal joint mechanism, Nature, 431 , 1062 (2004)

[145] S. Trachtenberg. The Cytoskeleton of Spiroplasma : A Complex Linear Motor, J. Mol. Microbiol. Biotechnol.11, 265 (2006); Shaping and moving a spiroplasma. J. Mol. Microbiol Biotechnol.7, 78 (2004);J. Kürner, A.S. Frangakis, W. Baumeister, Cryo-Electron Tomography Reveals the Cytoskeletal Structure of Spiroplasma melliferum. Science 21, 436 (2005);J.W. Shaevitz, J.Y. Lee & D.A. Fletcher. Spiroplasma Swim by a Processive Change in Body Helicity. Cell, 122, 941 (2005); H. Wada & R. R. Netz. Model for self-propulsive helical filaments: Kink-pair propagation. Phys. Rev. Lett. 99, 108102 (2007)

[146] A. Baumann, A. Sánchez-Ferrer, L. Jacomine, P. Martinoty, V. Le Houerou1, F. Ziebert and Igor M. Kulić, Motorized Fibers - The Material is the Wheel , Submitted manuscript (2017)

[147] (18) M.Yamada , et al., Photomobile Polymer Materials: Towards Light-Driven Plastic Motors, Angew. Chem. Int. Ed., 47, 4986 (2008);X. Zhang et al. Photoactuators and motors based on carbon nanotubes with selective chirality distributions, Nature Comm. 5, 2983 (2014)

[148] Michell, J.H.: On the stability of a bent and twisted wire. Messenger of Math. 11, 181–184, (1889–1990); A. Goriely, Twisted Elastic Rings and the Rediscoveries of Michell's Instability, J Elasticity (2006) 84: 281–299

[149] J. Goldstone, A. Salam, S. Weinberg: Broken Symmetries . Physical Review. 127, 965, (1962); P. C. Martin, O. Parodi, and P. S. Pershan, Unified Hydrodynamic Theory for Crystals, Liquid Crystals, and Normal Fluids, Phys. Rev. A 6, 2401 (1972) ; Chaikin, P., & Lubensky, T. Principles of Condensed Matter Physics. Cambridge: Cambridge University Press. (1995) ; Dieter Forster, Hydrodynamic Fluctuations, Broken Symmetry, and Correlation Functions, Advanced Book Classics, Addison-Wesley, 1990

[150] V. A. Vasiliev, Yu. M. Romanovskii, D. s. Chernavskii, v. G. Yakhno, Autowave Processes in Kinetic Systems , Spatial and Temporal Self-Organization in Physics, Chemistry, Biology, and Medicine. Berlin:

Springer Netherlands. 1987; A.W. Liehr Dissipative Solitons in Reaction Diffusion Systems, Springer 2013

[151] H.P. McKean, Nagumo's equation, Adv. Math. 4, 209 (1970)

[152] Mura, Toshio. Micromechanics of defects in solids. Vol. 3. Springer, 1987.